Science of the Total Environment 902 (2023) 166440

Contents lists available at ScienceDirect

Science of the Total Environment

journal homepage: www.elsevier.com/locate/scitotenv

Characterizing the sources of ambient PM_{10} organic aerosol in urban and rural Catalonia, Spain

Marten in 't Veld [a,b,*,1], Peeyush Khare [c,1], Yufang Hao [c], Cristina Reche [a], Noemi Pérez [a], Andres Alastuey [a], Jesús Yus-Díez [d], Nicolas Marchand [e], Andre S.H. Prevot [c], Xavier Querol [a], Kaspar R. Daellenbach [c,*]

[a] Institute of Environmental Assessment and Water Research, IDAEA-CSIC, Barcelona 08034, Spain
[b] Department of Civil and Environmental Engineering, Universitat Politècnica de Catalunya, Barcelona 08034, Spain
[c] Laboratory of Atmospheric Chemistry, Paul Scherrer Institute, Villigen 5232, Aargau, Switzerland
[d] Centre for Atmospheric Research, University of Nova Gorica, Vipavska 11c, SI-5270 Ajdovščina, Slovenia
[e] Aix Marseille Univ., CNRS, Marseille, France

HIGHLIGHTS

- Water-soluble OA concentrations were significantly higher in BCN compared to MSY.
- The relative compositions was similar between BCN and MSY, but OA sources differed.
- 5 common sources of organics were found in PM_{10}, three primary, and two secondary.
- SOA accounted for over 50 % of the OA at both stations.
- BCN was a mix of biogenic and anthropogenic SOA, while MSY was primarily biogenic.

GRAPHICAL ABSTRACT

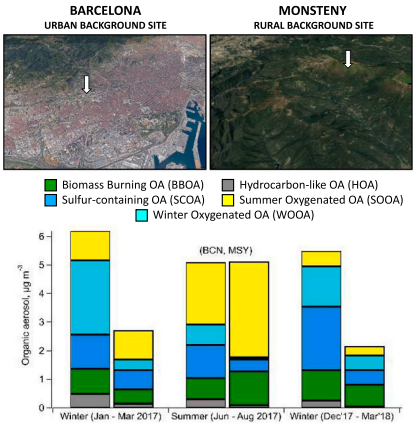

ARTICLE INFO

Editor: Hai Guo

Keywords:
PM10
Chemical composition
Organic aerosols
SOA
Source apportionment

ABSTRACT

Organic aerosols (OA) have recently been shown to be the dominant contributor to the oxidative potential of airborne particulate matter in northeastern Spain. We collected PM_{10} filter samples every fourth day from January 2017 to March 2018 at two sampling stations located in Barcelona city and Montseny Natural Park, representing urban and rural areas, respectively. The chemical composition of PM_{10} was analyzed offline using a broad set of analytical instruments, including high-resolution time-of-flight mass spectrometry (HR-ToF-AMS), a total organic carbon analyzer (TCA), inductively coupled plasma atomic emission spectrometry (ICP-AES), inductively coupled plasma mass spectrometry (ICP-MS), ion chromatography (IC), and thermal-optical carbon analyzer. Source apportionment analysis of the water-soluble organic content of the samples measured via HR-

* Corresponding authors.
E-mail addresses: marten.veld@idaea.csic.es (M. in 't Veld), kaspar.daellenbach@psi.ch (K.R. Daellenbach).
[1] These authors contributed equally to the manuscript.

https://doi.org/10.1016/j.scitotenv.2023.166440
Received 27 May 2023; Received in revised form 17 July 2023; Accepted 13 August 2023
Available online 21 August 2023

ToF-AMS revealed two primary and two secondary sources of OA, which included biomass-burning OA (BBOA), sulfur-containing OA (SCOA), as well as summer- and winter-oxygenated OA (SOOA and WOOA). The presence of hydrocarbon-like water-insoluble OA was also identified based on concentration trends in black carbon and nitrogen oxides. The results from the source apportionment analysis of the inorganic composition were correlated with different OA factors to assess potential source contributors. Barcelona showed significantly higher average water-soluble OA concentrations (5.63 ± 0.56 μg m^{-3}) than Montseny (3.27 ± 0.37 μg m^{-3}) over the sampling period. WOOA accounted for nearly 27 % of the averaged OA in Barcelona compared to only 7 % in Montseny. In contrast, SOOA had a greater contribution to OA in Montseny (47 %) than in Barcelona (24 %). SCOA and BBOA were responsible for 15–28 % of the OA at both sites. There were also seasonal variations in the relative contributions of different OA sources. Our overall results showed that local anthropogenic sources were primarily responsible for up to 70 % of ambient soluble OA in Barcelona, and regulating local-scale emissions could significantly improve air quality in urban Spain.

1. Introduction

Air pollution is the single largest environmental risk to public health worldwide (World Health Organisation (WHO), 2021). These health issues are primarily driven by exposure to high levels of airborne particulate matter (PM), which causes both short- and long-term health effects, such as cardiovascular and respiratory illnesses, cancer, and prenatal issues (Chen and Hoek, 2020; Mukherjee and Agrawal, 2017; WHO, 2021; Zhang et al., 2018a). PM <10 μm in aerodynamic diameter (PM_{10}) consists of a broad range of primary and secondary components (e.g., carbonaceous species, metals, and salts); the contributions of these sources vary at different locations (Bozzetti et al., 2017; in 't Veld et al., 2021; Jia et al., 2017; Querol et al., 2004a, 2004b, 2006, 2014; Vlachou et al., 2018; Zhang et al., 2018b). 10 – 40 % of PM_{10} is composed of organic aerosol (OA) that is either directly emitted into the atmosphere (primary organic aerosols; POA) or formed within the atmosphere via secondary oxidative processes (secondary organic aerosols; SOA) (Derwent et al., 2010; Kanakidou et al., 2005). Characterizing the chemical composition of PM_{10} is important for the interests of public health since metals (e.g. Fe, Cu, As, Cd, Ni, and V) and organic constituents (often associated with black carbon (BC)) are major drivers of PM_{10} toxicity (Chowdhury et al., 2019; Decesari et al., 2017; Delfino et al., 2010; Heal et al., 2012; Jia et al., 2017; Kelly and Fussell, 2012; Li et al., 2019; Park et al., 2018; Qi et al., 2020; Zhang et al., 2018a).

A considerable number of studies have investigated the sources of bulk PM, while others have identified the major sources of PM in both urban and rural areas in NE Spain (Amato et al., 2009b; Brines et al., 2019; Escudero et al., 2015; in 't Veld et al., 2021, 2023; Pandolfi et al., 2016; Querol et al., 2001, 2006, 2007). However, these datasets lacked information about OA speciation and only measured the total amount of organic carbon and elemental carbon (henceforth referred to as OC and EC, respectively). While the provenance of EC was mostly attributed to traffic emissions (Amato et al., 2009a; in 't Veld et al., 2021, 2023; Pandolfi et al., 2016), no clear source was identified for OC. This represents a significant gap in the literature: between 2009 and 2018, the relative contribution of OA to ambient PM —especially $PM_{2.5}$ — increased by 12 % and 9 % in urban and rural parts of the region, respectively (in 't Veld et al., 2021). Previous research focused on OA speciation in Barcelona, NE Spain, found that 60 – 80 % of ambient OA was formed via secondary pathways (Van Drooge et al., 2022; Via et al., 2021). Identifying the sources of secondary OA in this region is important, especially since OA was recently shown to be the dominant contributor to PM_{10} toxicity, significantly influencing the toxicity of fine particulates (in 't Veld et al., 2023). This requires an understanding of the chemical composition of OA in order to quantify the relative importance of air pollution sources, as well as constrain their impacts on the environment and public health.

In this study, we investigated the OA source contributions of PM_{10} in NE Spain by analyzing PM_{10} filter samples with a high-resolution time-of-flight aerosol mass spectrometer (HR-ToF-AMS), which has been widely used for the characterization of OA (Bozzetti et al., 2017; Crippa et al., 2014; Daellenbach et al., 2016, 2017; Huang et al., 2015; Srivastava et al., 2021; Vlachou et al., 2018). By constraining the sources of urban and rural OA in the Barcelona region, our work provides insights into the mitigation strategies that should be enacted in the area.

2. Materials and methods

2.1. Site description and sampling

PM_{10} filter samples were obtained from two stations in the conurbation of Barcelona in the western Mediterranean Basin (Fig. 1). One of the two stations is a rural background station located in a forested area in Montseny Natural Park (MSY; 41° 46' 45.63' 'N, 02° 21' 28.92" E; 720 m a.s.l.). The MSY station is located 50 km NNE of Barcelona and 25 km from the Mediterranean coast. This station is located at a sufficient distance and elevation such that it is unaffected by urban anthropogenic emission sources and has been shown to be representative of the regional ambient background (Minguillón et al., 2015; Pandolfi et al., 2016; Yáñez-Serrano et al., 2021). However, it can be affected by emissions from urban and industrial areas during anticyclonic atmospheric conditions; these conditions were not observed during this study (Cusack et al., 2012; Ealo et al., 2017, 2018; Gangoiti et al., 2001; in 't Veld et al., 2021, 2023; Millán et al., 1997, 2002; Pandolfi et al., 2013, 2014, 2016; Pérez et al., 2008; Pey et al., 2009; Ripoll et al., 2015). The MSY station is also part of the European Aerosols, Clouds, and Trace Gases Research InfraStructure Network (ACTRIS) and the Global Atmosphere Watch (GAW). The station located in Barcelona city at the Institute of Environmental Assessment and Water Research (IDAEA-CSIC) is an urban background air quality station (BCN; 41° 23′ 14.5″ N, 2° 06′ 55.6″ E; 68 m a.s.l.). It is situated close to Diagonal Avenue — one of the main traffic arteries of the city — and is surrounded by a broad range of commercial buildings (Amato et al., 2009a; Cusack et al., 2012; in 't Veld et al., 2021, 2023; Pandolfi et al., 2014, 2016; Pérez et al., 2008; Pey et al., 2009; Querol et al., 2004a, 2004b, 2014; Ripoll et al., 2015).

24-h (12.00 am – 11.59 pm) PM_{10} samples were collected at both stations every fourth day between January 2017 and March 2018. The samples were collected using DIGITEL DH80 high-volume samplers (30 m^3 h^{-1}) equipped with 15-cm diameter ultrapure quartz microfiber filters (PALL). Each filter sample was weighed before and after sampling; samples were stabilized for 48 h at 20 °C and 50 % RH to obtain the gravimetric PM mass. The sampled filters were subsequently cut into quarters for subsequent analysis.

2.2. Offline aerosol mass spectrometry

One portion of the filter sample was used to characterize the chemical composition of the OA using a high-resolution time-of-flight aerosol mass spectrometer (HR-ToF-AMS, henceforth shortened to AMS). The operating principles and calibration steps of the AMS instrument are described in (DeCarlo et al., 2006), while offline analysis protocols used can be found in (Daellenbach et al., 2016). In brief, 2 cm^2 punches of filter material were extracted in 10 mL ultrapure milliQ water (18.2 MΩ

cm, total OC > 5 ppb, 25 °C) by sonicating the samples at 30 °C for 20 min followed by 1 min of vortexing. The extracts were filtered using 0.45 μm nylon membrane syringe filters and spiked with known quantities of labeled ammonium nitrate ($NH_4^{15}NO_3$) and ammonium sulfate ($(NH_4)_2^{34}SO_4$) standards. The extracts were subsequently nebulized using an auto sampler (ESI) with synthetic air from the laboratory, dried with a Nafion diffusion dryer, and measured using the AMS at a 30-s time resolution. Each sample was nebulized for 8 min, which allowed for the collection of 16 mass spectra per sample. To minimize memory effects, milliQ water was nebulized for 6 min before each sample as a systematic blank. The AMS data was analyzed using high-resolution peak fitting procedures using the Squirrel v1.52L (SeQUential Igor data RetRiEvaL) and Pika v1.10C (PeakIntegration by Key Analysis, D. Sueper) modules in the IGOR Pro software package (Wavemetrics, Inc., Portland, OR, USA). Peaks were fitted to high-resolution data for each mass-to-charge ratio (m/z) in the range between 12 and 125. We also corrected for the interference of NH_4NO_3 in the CO_2^+ signal, previously described by Pieber et al. (2016) and presented in Eq. 1:

$$CO_{2,actual} = CO_{2,meas} - \left(\frac{CO_{2,meas}}{NO_{3,meas}}\right)_{NH_4NO_{3,pure}} * \left(NO_{3,meas} + j15NO_{3,meas}\right) \quad (1)$$

We added $j15NO_3$ to the equation to account for the labeled nitrate (containing the ^{15}N isotope) which we used as an internal standard for our sample extracts. The correction slope, $(CO_2/NO_3)_{NH4NO3,\ pure}$, was obtained by nebulizing five different concentrations of pure NH_4NO_3 and measuring their spectra using the AMS instrument. This slope only varied by ~2 – 3 % throughout the entirety of the measurement period.

2.3. Source apportionment of organic aerosol

The OA was source apportioned using positive matrix factorization (PMF). PMF describes the observed temporal dynamics in OA concentrations through linear combinations of the product of the static factor profiles ($f_{j,k}$) and their time-dependent contributions ($C_{k,t}$) with the residual matrix ($r_{j,t}$) as shown in Eq. 2.

$$C_{j,t} = \sum_{k=1}^{n} C_{k,t}.f_{j,k} + r_{j,t} \quad (2)$$

The index j represents an ion, t is a specific point in time and k is a factor. The input data and error matrices consisted of 302 distinct sample spectra acquired from AMS measurements, each with 300 organic fragment ions. Each row of the data matrix represents a sample-specific mass spectrum obtained from averaging the 10 mass spectra that showed the most consistent spectral features per sample in AMS measurements. The ultrapure milliQ water blanks that were nebulized before each sample were subtracted from the sample spectra. The sample-spectra were then normalized to their total signal intensity and scaled with the total water-soluble organic matter (OM) concentration (Eq. 3) to determine the ambient concentrations of fragment ions per sample.

$$C_{j,i} = \frac{x_{i,j}}{\sum_i x_{i,j}} * OC_i * \left(\frac{OM}{OC}\right)_i \quad (3)$$

Here, $C_{j,i}$ is the ambient concentration of fragment ion j in sample i, and OC and OM/OC are the sample-specific water-soluble OC concentrations and OM/OC ratio, respectively. The OC was measured using a

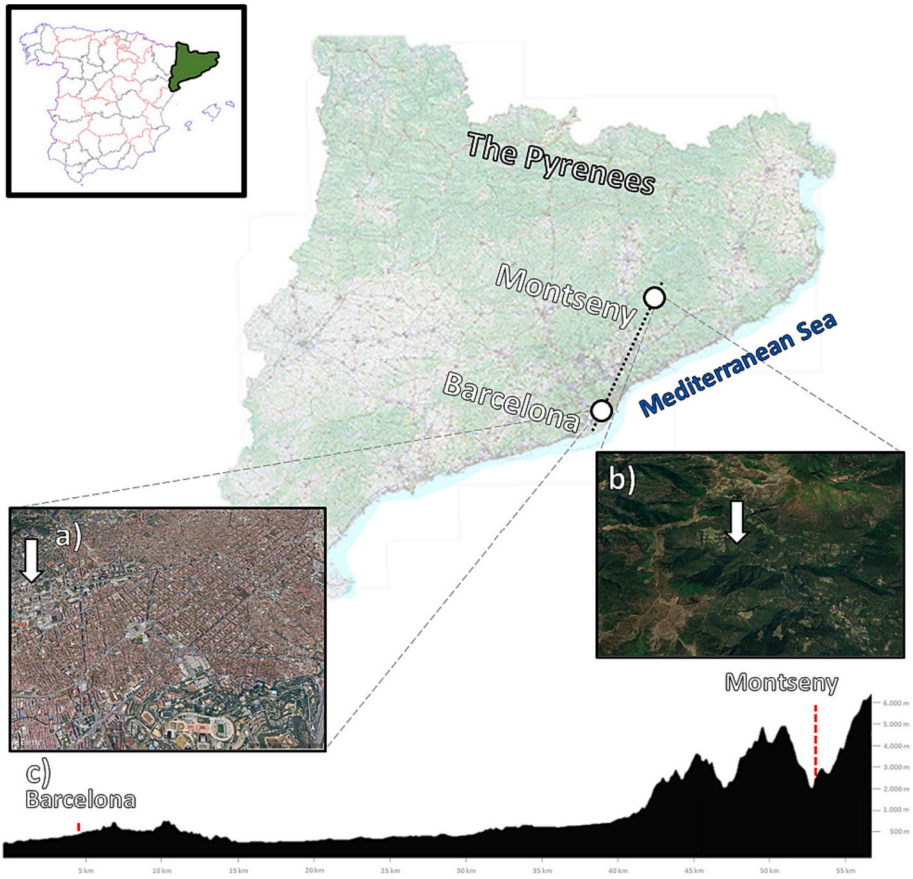

Fig. 1. Locations of the measurement stations in the Catalonia region of NE Spain where the sampling of PM10 was carried out. a) The location of the Barcelona urban (BCN) station (41° 23′ 14.5″ N, 2° 06′ 55.6″ E; 68 m a.s.l.). b) The location of the Montseny rural (MSY) station (41°46′45.63″N, 02°21′28.92″E, 720m a.s.l.). c) The topographic profile between BCN and MSY. Image credits: ©Google Earth & Institut Cartogràfic i Geològic de Catalunya (ICGC).

Shimadzu total OC analyzer and the OM/OC ratio was calculated from the AMS measurements. Uncertainties can be estimated from the input error matrix by calculating the standard deviation, accounting for variabilities in water blanks; the primary uncertainties in this experiment are associated with ion-to-ion signal variability at the detector as well as ion counting statistics. The calculation of the standard deviation ($s_{j,i}$) is shown in Eq. 4, where $C_{j,i}$ is the of fragment ion j in sample i; $C_{j,m}$ is the mean concentration, and n is the total number of samples.

$$s_{j,i} = \sqrt{\frac{\sum_{i=1}^{n} \left(C_{j,i} - C_{j,m}\right)^2}{n-1}} \quad (4)$$

We also observed that some of the AMS runs per sample were auto-correlated; we corrected for its enhancing effect on uncertainty by adjusting the number of runs per sample during the calculating of the standard deviation for the error matrix. The effects of autocorrelation on temporal measurements are described in detail in (Zięba and Ramza, 2011). Briefly, an auto-correlation coefficient (r_k) was first calculated and subsequently averaged over the concentrations of all species in a sample (X_i) at different lags (k, where $k = 1, 2, 3, \ldots n$) as follows (Eq. 5):

$$r_k = \frac{\sum_{i=1}^{n-k} (X_i - X_m)\,(X_{i+k} - X_m)}{\sum_{i=1}^{n} (X_i - X_m)^2} \quad (5)$$

r_k decreases with increasing k since the similarities reduce as the lag increases between samples. We identified the lag number, k, corresponding to the last positive value of r_k and denote it as n_c. Consequently, the effective sample count (n_{eff}) to be used for the calculation of the standard deviation can be determined as shown in Eq. 6:

$$n_{eff} = \frac{n - 2n_c - 1 + n_c(n_c+1)/n}{1 + 2\sum_{k=1}^{n_c} r_k} \quad (6)$$

The corrected standard deviation (s_c) can then be calculated based on the effective sample count (Eq. 7):

$$s_c = \sqrt{\frac{n_{eff}}{n_{eff}-1}} * s \quad (7)$$

Hence, the standard error (se_c) to be used as the input for the error matrices in the PMF model can be determined as follows (Eq. 8):

$$se_c = \frac{s_c}{\sqrt{n_{eff}}} \quad (8)$$

The PMF model was configured using the Source Finder toolkit (SoFi Pro v.8.0; Canonaco et al., 2021; Crippa et al., 2013a), developed in the Igor Pro software package (Wavemetrics, Inc., Portland, OR, USA). The PMF algorithm was solved using a multilinear engine-2 solver (ME-2 solver; (Paatero, 1999)) and an unconstrained source apportionment analysis was performed. The model was run for different numbers of factors until a solution with interpretable factors was identified. Factors contributing to the water-soluble OC were identified based on the extent of their explained variation of $C_2H_4O_2^+$ (for biomass-burning organic aerosol) and $CH_3SO_2^+$ (for sulfur-containing organic aerosol) ions, as well as winter–summer seasonality. Winter and summer seasonal factors were further correlated with typical secondary seasonal factors, such as inorganic nitrate and sulfate. 5- and 6-factor solutions were also investigated. However, these included additional, highly oxygenated factors that were not seasonal and showed unstable chemical profiles over several iterations. Furthermore, the mass spectra of these additional factors also did not have significant contributions from typical marker species (e.g., $C_2H_4O_2^+$). Finally, the 4-factor solution corresponding to water-soluble organic aerosol was selected, and bootstrapped over 2000 iterations to confirm the stability of the solution (Fig. S1).

2.4. Calculation of recovery fraction

As it is difficult to completely extract water-soluble OC from a filter sample, the recovery fractions for the water-soluble factors obtained from PMF analysis were calculated using the multilinear regression model shown in Eq. 9 and solved using a Stan model in Python:

$$\text{Total OC}_i - \text{HOC}_i \sim \text{Normal}\left(\frac{W_i}{\beta_i}, \sigma^2\right) \quad (9)$$

where Total OC_i represents total bulk OC measured in a filter sample, HOC_i is the hydrocarbon-like water-insoluble OC, W_i represents the individual water-soluble factors obtained from PMF analysis, β_i is the water recovery fraction of factor i ($0 < \beta < 1$), and σ^2 is the relative error of the measurements. To calculate the recovery (β_i) of each factor, the multivariate regressions were iterated over 400 times. Seasonal summer and winter secondary factors associated with SOA exhibited the highest recoveries, ranging between 65 and 85 %, while the sulfur-containing factor exhibited the lowest recovery (~20 %; Fig. S2).

2.5. Black carbon measurements and estimation of hydrocarbon-like organic carbon

The mass concentration and aerosol light absorption coefficient at seven different wavelengths (370, 470, 520, 590, 660, 880, and 950 nm) of BC were obtained using an aethalometer (Magee Scientific, USA, type AE33). Data were collected at both the BCN and MSY sites following procedures described in (Drinovec et al., 2015). Briefly, over the study period, samples were collected every 5 min on a TFE-coated glass filter tape. The aethalometer was then used to measure the transmission of seven different wavelengths of light through two sample spots (of which one was a reference spot). The mass of the BC was calculated based on the change in optical attenuation at 880 nm, a wavelength at which other aerosol particles exhibit significantly less absorption (Drinovec et al., 2015 and references therein). The parameters used to obtain the absorption and BC measurements were taken from Yus-Díez et al. (2021). Sandradewi et al. (2008) developed an aethalometer model that allowed for the source apportionment of the BC data using light absorption at 470 nm and 950 nm, which can be attributed to BC components originating from fossil fuels and the burning of biomass, respectively. Using this ratio, the fraction of BC originating from fossil fuel and wood burning could be determined; these fractions—as well as the BC concentrations obtained at 880 nm—were used to calculate the concentrations of both fossil fuel BC (BC_{ff}) and wood burning BC (BC_{wb}) (Alfoldy et al., 2023; Sandradewi et al., 2008). It should be noted that the aethalometer-based source apportionment model has been estimated to have an uncertainty of 35 % (Healy et al., 2017). The BC source apportionment was performed on the entire MSY dataset, but only on a subset of the BCN dataset (June 2017–March 2018) due to instrumentation issues between January and May 2017. Instead, the BC_{ff} at the BCN site during this period was estimated using NO_x data by extrapolating the linear relationship observed between BC_{ff} and NO_x during June 2017–March 2018 measurements (Fig. S3).

Hydrocarbon-like OC (HOC) was calculated from the concentration of fossil fuel-based EC using Eq. 10 (Casotto et al., 2022):

$$HOC_{EC,ff} = EC_{ff} \cdot \left(\frac{OA}{EC}\right)_{HOA} \cdot \left(\frac{OA}{OC}\right)_{HOA}^{-1} \quad (10)$$

where $(OA/EC)_{HOA} = 0.61$ (Crippa et al., 2013a; Healy et al., 2013) and $(OA/OC)_{HOA} = 1.24$ (Mohr et al., 2012); these values were both estimated from online measurements.

2.6. Auxiliary offline analytical techniques

The three remaining quarters of the filter samples were used to determine the chemical speciation. A 1.5 cm^2 subsample was punched

from one quarter and used to measure the OC/EC concentrations of the samples using a thermal-optical carbon analyzer (SUNSET) following the EUSAAR2 protocol (Cavalli and Putaud, 2010).

A second quarter was digested in acid (HNO_3:HF:$HClO_4$; 1:2:1) and analyzed using inductively coupled plasma atomic emission spectrometry (ICP-AES, ICAP 6500 Radial View, Thermo Fisher Scientific) to determine the concentration of major elements (i.e. Al, Ca, Cu, Fe, K, Mg, Mn, Na, P, and S), as well as inductively coupled plasma mass spectrometry (ICP-MS, iCAP-RQ, Thermo fisher Scientific), which was used to characterize a broader suite of trace elements (Li, Be, Sc, Ti, V, Cr, Mn, Co, Ni, Cu, Zn, Ga, Ge, As, Se, Rb, Sr, Y, Zr, Nb, Mo, Cd, Sn, Sb, Cs, Ba, La, Ce, Pr, Nd, Sm, Eu, Gd, Tv, Dy, Ho, Er, Tm, Yb, Lu, Hf, Ta, W, TI, Pb, Bi, Th, and U; Querol et al., 2001). The accuracy of the ICP-AES and ICP-MS measurements was assessed by analyzing 10 mg of a fly ash reference material (National Institute for Standards and Technology-1633b) loaded on a 150-mm blank filter (Amato et al., 2009a; Escrig et al., 2009). In cases where the detected chemical species could have multiple sources (e.g., sea salts and planetary crust), individual fraction contributions of such species were derived based on calculations described in more detail in Section S.1 of the SI.

The final quarter of the filter sample was leached in ultrapure MilliQ water to determine the concentration of ions present in the sample, including nitrate (NO_3^-), sulfate (SO_4^{2-}), and chloride (Cl^-), using ion chromatography (IC; Dionex Aquion, Thermo Fisher Scientific). The calculated Cl^- concentrations have previously been identified as unreliable due to a change in the detector which significantly affected the Cl^- concentrations (in 't Veld et al., 2021). Thus, the Cl^- measurements have been removed from the source apportionment analysis. The accuracy of the IC measurements was determined by performing a batch-wise quality control test for each batch containing ~7 samples. This protocol included the measurement of an instrument blank, a standard of known concentration, and a quality control sample, removing uncertainties related to instrument contamination and performance, and mass calibration. Finally, the concentration of NH_4^+ was determined using a specific electrode (ORION 9512HPBNWP ammonium selective electrode, Thermo Fisher Scientific) and a potentiometer (ORION 4-Star potentiometer, Thermo Fisher Scientific). The detection limits of different species were calculated as described by Amato et al. (2009a, 2009b) and Escrig et al. (2009) using Eq. 11:

$$LoD_j = 3*\frac{\sqrt{\sigma_a^2 + \sigma_{BLK}^2}}{V_j} \quad (11)$$

Here, the limit of detection of species *j* is calculated using the uncertainty associated with the analytical procedure, σ_a, the uncertainty of the blank measurements, σ_{BLK}, and the air volume sampled, V_j. The limit of detection of the ICP-AES, IC, and the thermal-optical carbon analyzer was determined to be 0.01 μg. The limit of detection of the ICP-MS was found to be 1.44E-5 μg for the relevant species.

The data from the auxiliary measurements was used to perform a source apportionment analysis using the U.S. Environmental Protection Agency's PMF v5.0 software (Norris et al., 2014). The exact methodology used is described in Section S.2 of the SI. To correlate the found sources with the sources obtained from the AMS a multilinear regression model was used as described in Section S.3. of the SI.

2.7. Analysis of wind trajectories and regional fire spots

2.7.1. Wind trajectories

The trajectories of air masses entering the Barcelona region during the sampling period were estimated using the FLEXPART v10.4 model (Pisso et al., 2019), which uses a Lagrangian approach to track the dispersion of individual particles. The model was initiated with 4000 aerosol tracer particles that were released from two receptor sites every hour. The model also calculated the backward trajectories of these aerosol particles, accounting for meteorological conditions. Meteorological data were obtained from the U.S. National Atmospheric and Oceanic Administration's Global Forecast System (GFS), which had a 1° x 1° spatial resolution. The model domain had a horizontal resolution of 0.1° x 0.1° with a vertical extent of 30,000 m. The model produced particle trajectory outputs at a 1-h time resolution. No chemical packages were invoked in the model. The output from FLEXPART simulations described the potential influences from any regional sources that overlapped with the wind trajectories prior to arriving at the receptor sites as a 4-D function of potential emission sensitivity (PES) (Stohl et al., 2007). We assumed that the atmospheric pollutants were primarily emitted from ground- or near-ground-based sources; thus, the effective PES was derived from a so-called footprint layer (defined as 0–300 m in this study) and summarized as done in previous studies (Hüser et al., 2017; Lal et al., 2014).

2.7.2. Fire spots

The spatial distribution of open-fires (including wildfires and wood- and biomass-burning emissions) around the receptor sites during our sampling period was investigated using the information from the Visible Infrared Imaging Radiometer Suite (VIIRS) sensor on the Suomi National Polar-orbiting Partnership (S-NPP) satellite (EarthData, 2021). The distribution of fire spots was plotted over a regional map to assess the influence of wood- and biomass-burning events on the samples collected from the two measurement locations used in this study.

3. Results and discussion

3.1. Source contributions to bulk PM_{10} in Barcelona and Montseny

The average PM_{10} urban background concentration at the urban BCN station (16.1 ± 7.17 μg m^{-3}) was ~2 times higher than at the rural MSY station (8.5 ± 4.24 μg m^{-3}) (Fig. 2). It should be noted that there were no days that exceeded the European standard of 50 μg m^{-3} (EC, 2008, 2011). The bulk organic composition revealed that the sum of the OM and EC constituted 36 % of the PM_{10} collected at BCN, which was slightly lower than their average contribution to the MSY PM_{10} (42 %), likely due to the diverse urban source contributions at BCN. Secondary inorganic aerosols (BCN: 30 %; MSY: 28 %) and mineral aerosols (BCN: 25 %; MSY: 26 %) were also important sources with comparable contributions at both locations. Sea spray aerosols (BCN: 7 %; MSY: 4 %) had a slightly greater contribution to the PM_{10} measured at the BCN site due to its proximity to the coast as well as its lower altitude relative to the mean sea level. Additional calculations with tracer inorganic species for select subgroups are reported in Section S.1 of the SI. Other minor inorganic contributions identified during source apportionment included trace elements (BCN: 1 %; MSY: 0 %) and biomass burning (BCN: 1 %; MSY: 0 %). These results suggest that the PM_{10} composition, especially the inorganic chemical species and the bulk organics, was very similar between the two stations. This was consistent with the source apportionment of the inorganic fractions (described in detail in Sections S.2 and S.4 of the SI), which identified nine common sources between the two stations: these included aerosols derived from an OC-rich source, secondary sulfates, secondary nitrates, combustion, road dust, heavy oil, industry, mineral, and sea spray (Figs. S4-5). It is important to note that the PMF analysis of inorganic and bulk organic constituents was not sufficient to isolate biomass-burning as a distinct source due to the absence of specific biomass-burning tracers such as levoglucosan and monosaccharide anhydrides. A more detailed investigation of the contributions of biomass-burning based on AMS measurements is presented in Subsections 3.2.1.

3.2. OA source contributions in Barcelona and Montseny

The OA concentrations at BCN and MSY exhibited significant seasonal differences (Fig. 3a). The highest concentrations observed at BCN occurred during the winter, which exceeded summertime values by a

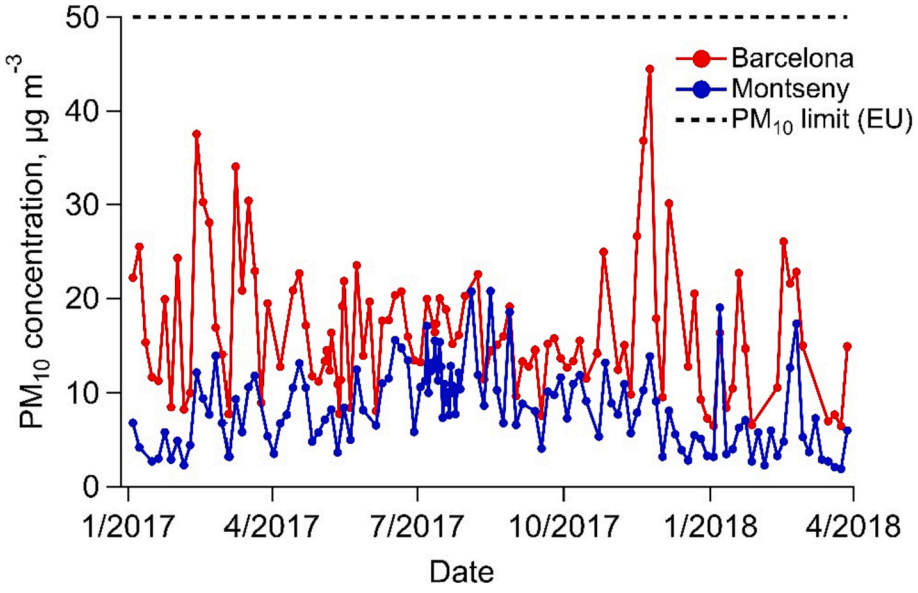

Fig. 2. Time series data of the PM10 concentrations (in µg m-3) at Barcelona (BCN) and Montseny (MSY) sites between January 2017 and March 2018. The dashed line indicates the acceptable ambient concentration limit for PM10 set by the European Union (EU) (EC, 2008).

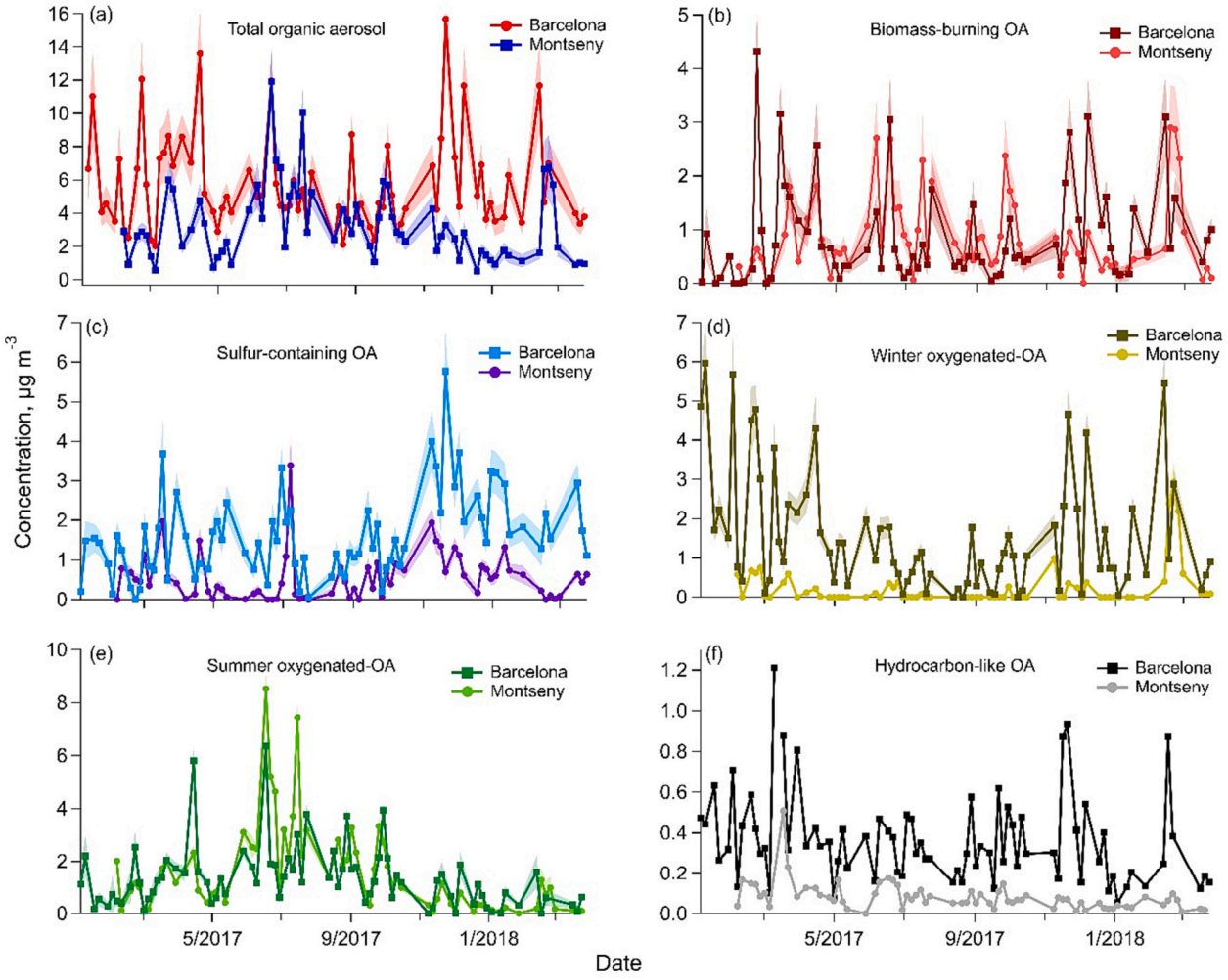

Fig. 3. Time series of the (a) total OA concentration and (b-f) the contributions of five different factors to the total OA observed at the Barcelona and Montseny measurement stations between January 2017–March 2018.

factor of three. In contrast, MSY exhibited the opposite seasonal trend, with OA peaking during summer (June – August 2017) and decreasing by a factor of ~2 – 3 during the winter. Overall, the average OA at BCN (5.63 ± 0.56 μg m^{-3}) was significantly higher than at MSY (3.27 ± 0.37 μg m^{-3}) over the entirety of the sampling duration. Source apportionment analysis revealed four factors contributing to the water-soluble OA mass (Fig. 3b–e). Based on the distinct mass spectra attributed to each factor, these were identified as sulfur-containing OA (SCOA), biomass-burning OA (BBOA), summer oxygenated OA (SOOA), and winter oxygenated OA (WOOA) (Fig. 4). We note that SOOA and WOOA were named based on significant seasonal enhancements in their contributions to water-soluble organic aerosol, yet they were not limited to specific seasons. In addition, a hydrocarbon-like water-insoluble organic aerosol (HOA) factor was also identified based on traffic-related EC and NO_x measurements using Eq. 10 (Fig. 3f, S1). Upon accounting for the recovery fractions, the total OC that could be attributed to these factors summed to the separately measured bulk OC concentrations in our filter samples (Fig. S6), suggesting that our OC measurements achieved mass balance. These factors were classified into primary (BBOA, SCOA, and HOA) and secondary (SOOA and WOOA) and are discussed in detail in Subsections 3.2.1 and 3.2.2.

3.2.1. *Primary OA*

3.2.1.1. Biomass-burning OA. BBOA was identified based on the prominence of the $C_2H_4O_2^+$ (m/z 60) and $C_3H_5O_2^+$ (m/z 73) ions in the AMS spectra, which are chemical fingerprints of levoglucosan (Daellenbach et al., 2017). Levoglucosan is produced from the pyrolysis of cellulose and is a tracer for biomass-burning sources (Alfarra et al., 2007; Crippa et al., 2013b; Daellenbach et al., 2018; Via et al., 2021; Zotter et al., 2014). BBOA mass spectra exhibited an OM:OC ratio of 2.07 as well as a f_{44}:f_{60} ratio of 5 with a f_{44} value of 0.07, suggesting fresh emission

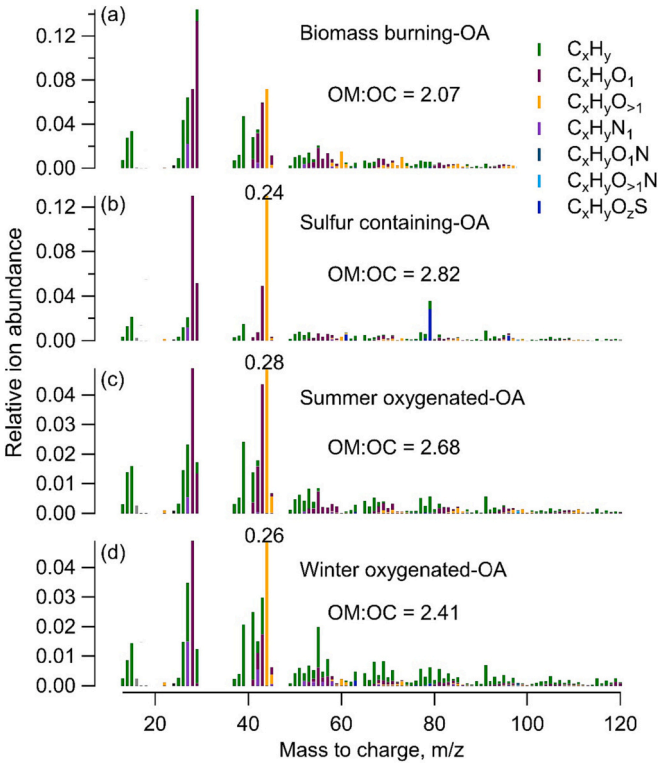

Fig. 4. Mass spectra of the (a) BBOA, (b) SCOA, (c) SOOA, and (d) WOOA sources as determined by the source apportionment of the water-soluble fraction of PM10 organic aerosol. Note: The numbers on individual mass spectra show the maximum value of the m/z 44 ion signal on each spectrum.

contributions. BBOA exhibited some seasonal variations at the BCN site, where it peaked during winter but exhibited relatively reduced summertime signals. Furthermore, the wintertime BBOA remained consistently higher at BCN than at MSY. Our results suggest that local-scale anthropogenic sources (e.g., wintertime domestic heating via wood burning) could be a major source of BBOA at BCN (Minguillón et al., 2011; Mohr et al., 2012; Viana et al., 2013). An analysis of the wind trajectories of air masses crossing into BCN also showed significantly reduced atmospheric transport during winter, supporting our hypothesis that wintertime BBOA was mostly dominated by local sources that originated within the local urban environment (Fig. 5).

The BBOA trends at MSY were the opposite of those observed at BCN, with higher BBOA levels observed during summer compared to winter. The lower BBOA concentrations during winter could be attributed to meteorological effects, specifically the change in the height of the boundary layer. The MSY measurement station is located 720 m a.s.l. in Montseny Natural Park, which is characterized by mountainous terrain (Fig. S7) and remains mostly above the well-mixed boundary layer during winter months, which prevents the transport of anthropogenic pollutants from the BCN region to the MSY site. However, the boundary layer reaches the MSY sampling station in summer, resulting in improved mixing that vertically extends to the site, resulting in a higher BBOA signal between June – August 2017 (Minguillón et al., 2015; Pandolfi et al., 2013; Pey et al., 2010). It is also important to note that the summertime BBOA observed at BCN and MSY were comparable, indicating common source contributions at both locations. Since residential wood burning for heating is limited to winter periods, a likely source of summertime BBOA was open fires, especially regional wildfire events, which, owing to atmospheric mixing, would have affected both measurement stations. This is consistent with the increased number of open fire events near BCN and MSY between May – September 2017 relative to the winter period of that year, as well as the broader regional influence of air parcels arriving at the sampling locations (Fig. 5). The peak BBOA readings at MSY exceeded that observed at BCN on several days during the summer periods, likely due to the proximity of the MSY station to regional wildfires that affected forested areas. The BBOA at BCN was most strongly correlated with potassium ion (K^+) concentrations that are frequently emitted from wood-burning activities (Figs. S8–9). The BBOA at MSY was also relatively well-correlated with the total OC as well as ammonium and secondary sulfate, which was probably due to their similar seasonal prevalence in the atmosphere. At BCN, BBOA had a relatively high contribution to ambient OA concentrations (up to 30 %), but only had a 10 % contribution on less polluted days (Fig. S10a). However, at MSY, ambient OA concentrations were consistently composed of 20 – 35 % BBOA (Fig. S10b). When averaged over the entire sampling period, BBOA accounts for 15 ± 5 % of OA at BCN and 26 ± 8 % at MSY, with comparable concentrations at both sites (BCN: 0.84 ± 0.26 μg m^{-3}; MSY: 0.85 ± 0.26 μg m^{-3}). Via et al. (2021) found that BBOA exhibited similar relative contributions to PM_1 (relative contribution of 6 % of OA at BCN). The concentrations were significantly lower with 0.2 μg m^{-3} due to the smaller PM size.

3.2.1.2. Hydrocarbon-like OA. HOA accounted for 4 – 6 % of the total OA at BCN and MSY, which was comparable to previously published HOA contributions to the OA in PM_{10} (3 – 15 %) in other areas of Europe (Bozzetti et al., 2016, 2017; Casotto et al., 2022; Daellenbach et al., 2016, 2017, 2020; Qi et al., 2020; Vlachou et al., 2018). However, this was much lower than its relative contribution to PM_1, which was 12 % (Via et al., 2021).

The average HOA concentration at BCN (0.36 μg m^{-3}) was three times higher than at MSY (0.12 μg m^{-3}). Furthermore, HOA concentrations exhibited some seasonality at BCN, with concentrations spiking during the winter, but no significant seasonal trends were observed at MSY. In winter, the urban environment around BCN accounts for the very strong correlations between HOA, traffic, and road dust PMF sources ($r > 0.9$

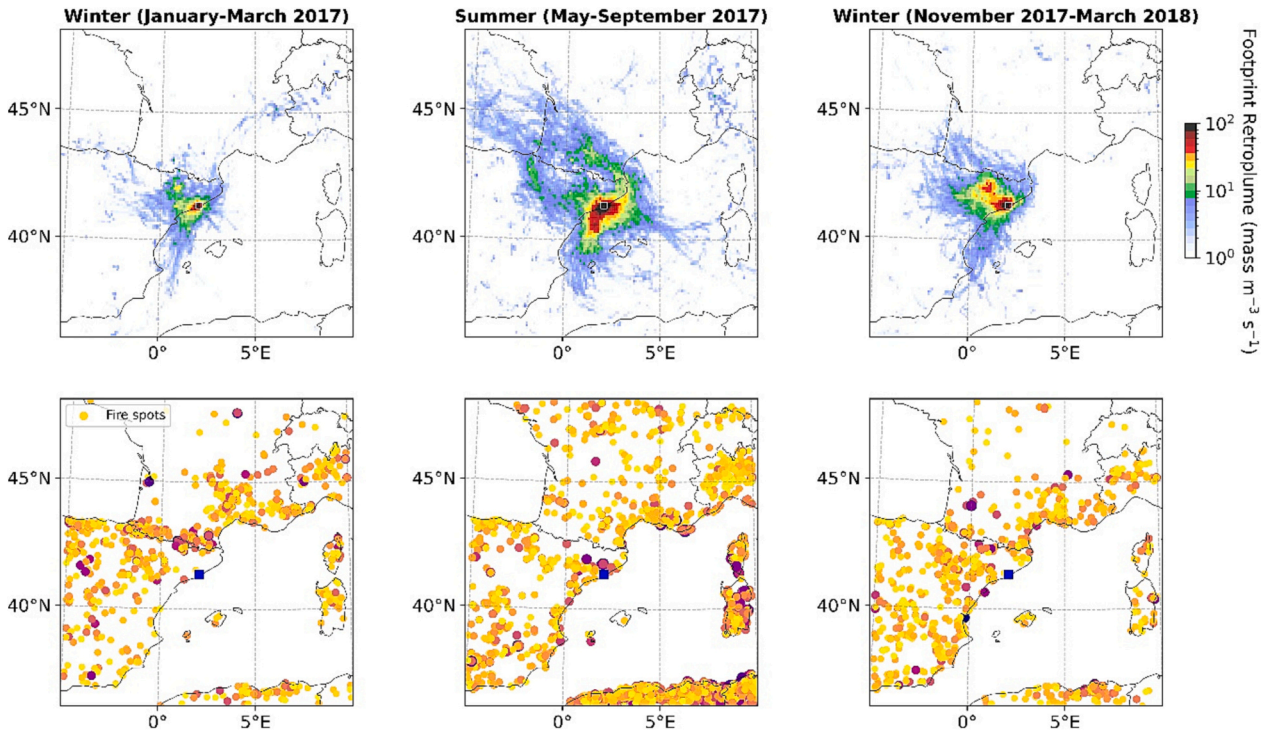

Fig. 5. The regional influence of open fires at the Barcelona and Montseny sampling stations based on incoming wind trajectories (a-c: FLEXPART v10.4) during (a) winter 2017, (b) summer 2017, and (c) winter 2018. (d-f) Total open-fire instances in Catalonia over each seasonal period based on satellite data. Note: In each panel, the blue squares represent the location of Barcelona city. Panels d-f magnify the eastern-most parts of Spain to focus on open-fires in areas near sampling stations estimated by wind trajectories.

over the entire year), as well as the correlation between EC and their respective tracer metal species (Fe, Cr, Cu, Sn, and Sb), consistent with the idea that mobile sources are major contributors of HOA in Barcelona city (Figs. S8–9). However, the HOA concentrations at MSY were comparatively less well-correlated with tracers of traffic-related sources and road dust during both winter and summer periods (r = 0.6 – 0.7). This was likely due to the spatial separation between the rural MSY station and the high density of urban mobile sources surrounding BCN.

3.2.1.3. Sulfur-containing OA (SCOA). SCOA exhibited a high OM:OC ratio of 2.82 and was identified during source apportionment based on the presence of $CHSO^+$ (m/z 61) and $CH_3SO_2^+$ (m/z 79) in its mass spectra. These ions have been previously shown to originate also from sources other than methane sulfonic acid (MSA), which is a tracer for marine sources (Bozzetti et al., 2017; Daellenbach et al., 2017, 2020; Vlachou et al., 2018). SCOA was the dominant contributor at BCN and accounted for 28 ± 6 % (1.59 ± 0.35 μg m^{-3}) of the measured OA on average. However, it contributed up to 70 % of the OA mass at BCN on days with low ambient OA concentrations (Fig. S10a). Its magnitude was considerably lower at MSY (0.56 ± 0.17 μg m^{-3}), though it still accounted for 17 ± 5 % of the measured OA. SCOA can originate from a variety of sources, ranging from primary non-exhaust traffic emissions, such as the resuspension of road dust containing tire wear, which is an important vehicle-related source of PM_{10} (Amato et al., 2009a, 2009b), to the secondary atmospheric processing of various precursor emissions (Daellenbach et al., 2020; Qi et al., 2020). The significant correlations (r = 0.5 – 0.7) between SCOA, road dust and mineral-related factors at BCN further support this observation (Figs. S8–9). We also confirmed the statistical significance of these correlations via p-value tests at individual sites and for a combined dataset, which showed $p < 0.05$ for all scenarios. No significant correlations were observed with other sectors (i.e. heavy oil, industry, traffic or sea spray sources) (Fig. S8). Moreover, size-resolved measurements in Barcelona showed that $CH_3SO_2^+$ concentrations in PM_{10} samples were 2 – 10 times higher than in PM_1 samples that were collected on selected few days across the sampling period. One would expect MSA to be mostly present in fine mode. So the appearance in the coarse mode is more consistent with tire wear-laden road dust resuspension being an important contributor to SCOA (as proposed in Daellenbach et al. (2017) for Swiss sites), although some contribution from MSA is not ruled out due to proximity of Barcelona to the coast. In addition, its poor correlations with EC, secondary sulfate, and total sulfate measurements suggest that the SCOA recorded at BCN was not influenced by traffic-related tailpipe emissions and inorganic sulfate. SCOA exhibited a stronger correlation with road dust at MSY during winter periods (r = 0.7 – 0.9). The strong correlation with road dust suggests that the non-exhaust contribution from mobile sources was more important in MSY, whereas the strong correlation between SCOA and the aforementioned sources at BCN suggests that SCOA may, in general, originate from a variety of sources.

3.2.2. Secondary OA

3.2.2.1. Summertime oxygenated OA (SOOA). The SOOA factor was named based on seasonality, as it had significantly enhanced contributions to OA concentrations in summer that correlated with an increase in other prominent summertime chemical species (e.g., secondary sulfate). However, its contributions to OA, though minor, were also observed in other seasons. Seasonality as a differentiation technique has also been applied in previous offline AMS studies (Bozzetti et al., 2016; Daellenbach et al., 2017). The mass spectra of SOOA was characterized as highly oxidized aerosol with an OM:OC ratio of 2.68; over 25 % of the ion signal could be attributed to the CO_2^+ fragment ion. While SOOA and WOOA had comparable CO_2^+ signals, the $CO_2^+/C_2H_3O^+$ ratio of SOOA (~7) was significantly lower than that of WOOA (~14), suggesting that SOOA was less aged than WOOA. This could be due to the increased magnitude of precursor biogenic emissions under higher temperature summertime conditions, which can relatively easily partition into the particle phase with some degree of oxidation (Canonaco et al., 2015; Daellenbach

et al., 2017). Previous ambient measurements have reported production of semi-volatile oxygenated organic aerosol during summer with similar or lower f_{44} values than winter but higher f_{43}, which is consistent with our measurements (Canonaco et al., 2015). SOOA was the largest contributor to OA at MSY with an average concentration of 1.51 ± 0.18 μg m^{-3}, accounting for 46 ± 6 % of the OA concentration observed at that station compared to its 24 ± 4 % contribution at BCN (1.33 ± 0.23 μg m^{-3}). It accounted for up to 75 % of the total ambient OA mass at MSY on relatively polluted days. On a few of the most polluted days, BBOA and SOOA collectively accounted for nearly all of the OA concentrations observed (Fig. S10b). However, SOOA had a comparatively modest contribution to OA concentrations at BCN (20 – 50 %). SOOA increased exponentially with the temperature at MSY, and the measured total OC was strongly correlated with SOOA during the summer periods ($r > 0.8$). This suggested that summertime increases in SOOA concentrations at MSY could be attributed to enhanced photochemical effects coupled with the increased emissions of terpenes and other biogenic VOCs in summertime conditions (Minguillón et al., 2011; Pérez et al., 2008; Querol et al., 2009, 2013; Rodríguez et al., 2002; Seco et al., 2011). Overall, given its exponential relationship with temperature, SOOA at MSY was dominated by biogenic secondary OA formation (bSOA) (Fig. 6), which is consistent with previous observations at other, similar locations (Bozzetti et al., 2017; Canonaco et al., 2015; Daellenbach et al., 2016; Leaitch et al., 2011; Vlachou et al., 2018).

We also evaluated the SOOA at BCN against the ambient temperature reported at MSY. This comparison was justified because while the ambient temperature of Barcelona city is influenced by low tree cover and the urban heat island effect, most biogenic sources in the region are located in the mountains, where temperatures would be more consistent with MSY than BCN. The SOOA at BCN also showed an exponential increase with the temperature recorded at MSY and was consistent with the previously reported temperature-dependence of bSOA by Leaitch et al. (2011) (Fig. 6). This suggested that the SOOA at BCN likely also originated from regional biogenic sources. Furthermore, SOOA time series data at both BCN and MSY were strongly correlated, suggesting common source contributions. However, SOA from other precursor emissions promoted by enhanced photochemical oxidation during the summer could also contribute to SOOA (Fig. S2).

3.2.2.2. Wintertime oxygenated OA (WOOA). The WOOA factor was also named based on seasonality with significantly enhanced wintertime contributions to ambient OA, and minor contributions at other times during the sampling period. WOOA showed slightly lower OM:OC ratio of 2.41 compared to SOOA, and remained higher at BCN than at MSY throughout the year. It had an average concentration of 1.51 ± 0.27 μg m^{-3} (27 ± 5 % of average PM_{10} organic mass concentration) at BCN, which exceeded the average 0.23 ± 0.05 μg m^{-3} (7 ± 2 %) measured at MSY. The wintertime WOOA concentrations at BCN ranged between 0.1 and 6 μg m^{-3}, with peak concentrations between four to eight times higher than those observed in summer. WOOA accounted for up to 50 % of ambient OA mass at BCN on more polluted days (Fig. S10a); indeed, WOOA and BBOA were responsible for 60 – 70 % of OA on polluted days at BCN. A different seasonal variation was observed at MSY, which exhibited negligible summertime WOOA concentrations (ranging between 0 and 1 μg m^{-3}) compared to winter peaks of ~2.5 μg m^{-3} (Figs. 3, S1). Our results suggest that WOOA originates from SOA sourced from local urban anthropogenic precursor emissions, which have a very limited influence at MSY due to reduced vertical mixing in wintertime conditions. Furthermore, the WOOA mass spectra exhibited some $C_2H_4O_2^+$ signals, which, coupled with high f_{44}, suggested the influence of aged biomass-burning emissions, consistent with seasonal household heating patterns. A reasonable correlation (r: ~0.6) between WOOA and biomass-burning-related BC during winter further supports the influence of biomass burning at the BCN site (Fig. S9). However, it should be noted that this correlation was not observed at MSY, likely due to meteorological effects. WOOA at BCN and MSY were also well-correlated with secondary nitrate (r: ~0.7) as well as other trace elements (Fig. S8–9), supporting an anthropogenic interpretation of SOA sources. WOOA and SOOA were also both highly aged with comparable f_{44} values, though some differences in mass spectra were observed: SOOA possessed greater contributions from $C_xH_yO^+$ and $C_xH_yO^+_{>2}$ fragments relative to WOOA across its spectrum, indicating a larger contribution of freshly formed SOA during summertime conditions. For example, SOOA exhibited a $C_3H_5^+$:$C_2H_3O^+$ fragment ratio of 3 at m/z 41; this same ratio had a value of 11 in WOOA. Similarly, the entire m/z 43 signal in SOOA could be attributed to $C_2H_3O^+$; this was in comparison to a relative contribution of 60 % in the WOOA mass spectra, with the remaining 40 % attributed to $C_3H_7^+$. The temporal variations in WOOA at both measurement locations suggested that anthropogenic sources contributed more to WOOA at the urban BCN site, while the OA concentrations at the rural MSY site were driven more strongly by regional highly aged aerosol during winter, with only a limited influence from anthropogenic sources located in Barcelona.

3.2.2.3. Importance of OA sources. The sum of the OM and EC contributions accounted for a significant fraction (36 – 42 %) of the bulk PM_{10} composition at both sites over the entire sampling period (Fig. 7a, 7b). The OM comprises three primary (HOA, BBOA, and SCOA) and two secondary (SOOA and WOOA) factors. When averaged over the sampling period, the BBOA (BCN: 0.84 ± 0.26 μg m^{-3}; MSY: 0.85 ± 0.28 μg m^{-3}) and SOOA (BCN: 1.33 ± 0.23 μg m^{-3}; MSY: 1.51 ± 0.18 μg m^{-3}) concentrations were comparable at both stations (Fig. S10c). However, BBOA had a relatively larger contribution at MSY (26 %) relative to BCN (15 %) due to the increased influence of diverse sources at BCN. HOA, SCOA, and WOOA together accounted for 3.46 ± 0.44 μg m^{-3} of the OA at BCN, significantly exceeding their 0.91 ± 0.17 μg m^{-3} contribution at MSY. This difference can be attributed to the differences in urban and rural conditions, with BCN more influenced by local anthropogenic

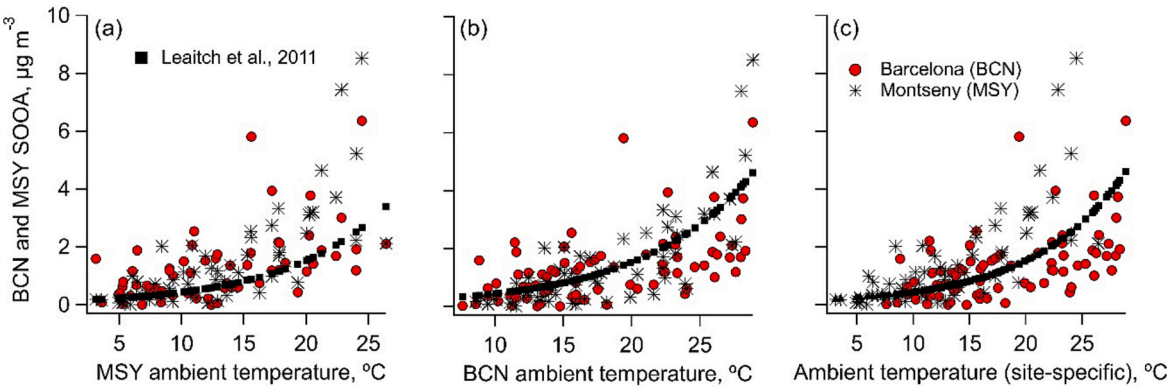

Fig. 6. Variation in BCN and MSY SOOA concentrations with ambient temperature measured at (a) Montseny, (b) Barcelona, and (c) individual sites.

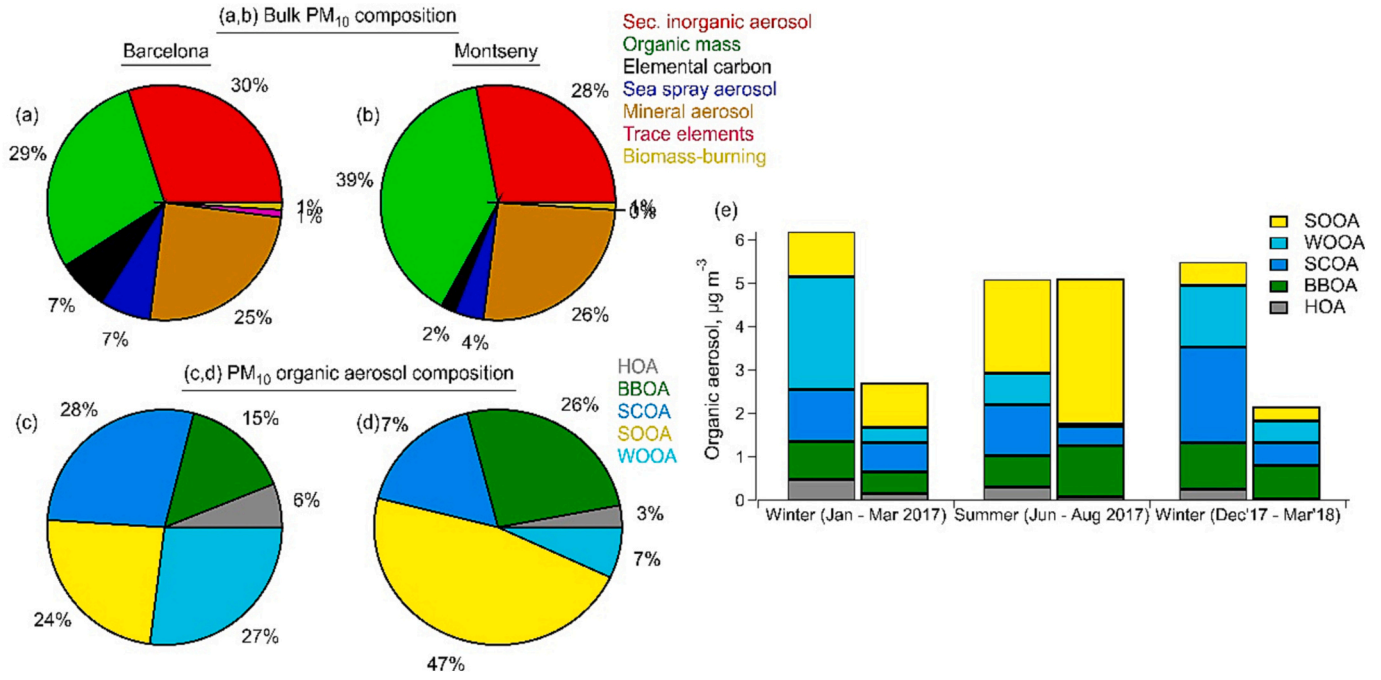

Fig. 7. The relative source contributions to (a, b) bulk PM10 mass chemical composition and (c, d) organic aerosol averaged over the entire measurement period (Jan 2017–March 2018) for the Barcelona (BCN) and Montseny (MSY) sites as determined by PMF-based source apportionment analysis. (e) Seasonally averaged source contributions to total organic aerosol at Barcelona and Montseny. Note: The two columns in (e) correspond to BCN and MSY measurements in the left and right columns, respectively.

sources relative to MSY; this also resulted in winter-averaged OA concentrations at BCN exceeding those observed at MSY by >100 %. However, the summer-averaged OA concentrations were comparable at both stations, though it should be noted that the relative source contributions were different at each station (Fig. 7e). The increased summertime OA concentrations at MSY could be primarily attributed to SOOA, which was strongly impacted by bSOA. In contrast, the summertime SOOA at the BCN site was comparatively less dominant due to its distance from the biogenic sources of SOOA, which were concentrated at higher altitudes (Fig. S7). The increased vertical convective transport during summer likely restricted their influence in low-lying areas; thus, SOOA was more prominent at MSY than BCN during this period.

At both stations, WOOA and SOOA were found to have contributed nearly half of the total OA mass (BCN: 51 %; MSY: 54 %) over the sampling period. This is only slightly lower than PM_1 studies conducted in BCN, which estimated that 60 % of the total OA could be attributed to SOA (Via et al., 2021). These contributions were mostly driven by SOOA (46 %) at the MSY site, while SOOA (24 %) and WOOA (27 %) both made comparable contributions at the BCN site (Fig. 7c-d). SCOA was the single largest contributor (28 %) to OA at BCN but had a reduced contribution at MSY (17 %), likely due to reduced non-exhaust traffic sources at MSY. The HOA was the lowest contributor to OA at both stations (BCN: 6 %; MSY: 4 %).

4. Conclusion and future work

We characterized the sources of OA in Catalonia accounting for the differences between urban (Barcelona) and rural (Montseny) regional influences. While the relative chemical composition of PM_{10} was similar at both the urban and rural stations, significant differences were observed in the OA composition at each station. While traffic-related sources and wood burning were the primary sources of EC, the OM originated from a variety of primary and secondary sources, including biomass-burning, sulfur-containing, and biogenic emissions. Among these, biomass-burning emissions associated with residential heating were the dominant contributions to OA in Barcelona, especially during winter when vertical mixing was typically restricted by low boundary layer conditions. During the summer, regional wildfires became important sources of BBOA; these were capable of influencing the OA at the MSY site due to enhanced vertical mixing under warmer conditions as well as the closer proximity of the MSY station to wildfire events. The SOOA component was likely related to biogenic precursor emissions due to its summer seasonality and its exponential relationship with the temperature at both stations, which are typical features of biogenic emissions. The rural MSY site exhibited larger SOOA contributions and was thus more strongly influenced by biogenic OA due to its closer proximity to the biogenic sources that were concentrated in the mountains in this region, as well as its separation from primary urban sources. In contrast, WOOA exhibited strong seasonal variations, especially in winter, and was identified to be of secondary anthropogenic origin due to its correlation with secondary. Our overall results show that the OA concentrations at BCN can be effectively reduced by regulating the anthropogenic emissions within the city, such as wood burning. This is because most of the wintertime OA sources at BCN were judged to be local, and consequently had a very limited influence on wintertime measurements at MSY.

OA-focused regulatory policies are also likely to have a positive impact on public health since several studies have linked the oxidative potential of ambient aerosol to its oxygenated anthropogenic organic constituents. However, effective policies require a detailed understanding of different OA sources. In this study, we successfully identified primary and secondary contributors to OA; however, the sources contributing to SOA in this region need to be further constrained in future work, such as by investigating the chemical composition of OA at the molecular level. For example, a previous study found that cooking-related OA contributed 14 – 18 % to OA (accounting for source-specific relative ionization efficiencies around 10 %) (Via et al., 2021), while such organic aerosol was not identified in the present analysis. Given the relatively small contribution to OA and its limited solubility, cooking-related OA is likely mixed with other urban OA sources here. Alternatively, filter sampling at higher time resolutions (e.g., 12-h

samples) would capture diurnal variations in OA composition, which can be used to investigate the role of the different SOA formation processes. Online and offline gas-phase measurements can also be used to identify precursor emissions leading to the formation of SOOA and WOOA, especially given their large contribution (~50 %) to the total OA mass in PM_{10}. Finally, the relative importance of different OA sources can be established by the characterization of the chemical speciation of $PM_{2.5}$ and PM_1, since certain factors (e.g., SCOA) are more prevalent in larger particles but have minimal contributions to $PM_{2.5}$ (Daellenbach et al., 2020; Qi et al., 2020).

CRediT authorship contribution statement

Marten in 't Veld: Software, Formal analysis, Writing – original draft, Writing – review & editing, Visualization. **Peeyush Khare:** Methodology, Software, Formal analysis, Writing – original draft, Writing – review & editing, Visualization, Funding acquisition. **Yufang Hao:** Formal analysis, Software. **Cristina Reche:** Validation, Data curation. **Noemi Pérez:** Validation, Data curation. **Andres Alastuey:** Conceptualization, Methodology, Resources, Supervision, Funding acquisition. **Jesús Yus-Díez:** Formal analysis, Data curation. **Nicolas Marchand:** Resources, Supervision. **Andre S.H. Prevot:** Conceptualization, Methodology, Resources, Supervision, Funding acquisition. **Xavier Querol:** Conceptualization, Methodology, Resources, Supervision, Project administration, Funding acquisition. **Kaspar R. Daellenbach:** Conceptualization, Methodology, Resources, Supervision, Project administration, Funding acquisition.

Declaration of competing interest

The authors declare that they have no known competing financial interests or personal relationships that could have appeared to influence the work reported in this paper.

Data availability

Data will be made available on request.

Acknowledgments

This study was supported by the European Union's Horizon 2020 research and innovation program under grant agreement 101036245 (RI-URBANS), the "Agencia Estatal de Investigación" from the Spanish Ministry of Science and Innovation, European Regional Development Fund (FEDER) funds under the projects CAIAC (PID2019-108990RB-I00), the Generalitat de Catalunya (AGAUR 2021 SGR 00447), and the Direcció General de Territori. P.K. also acknowledges support from the European Union's Horizon 2020 research and innovation CoFund program under grant agreement no. 884104 (Marie S. Curie Actions). K.R. D. acknowledges support from the Swiss National Science Foundation Ambizione grant PZPGP2_201992.

Appendix A. Supplementary data

Supplementary data to this article can be found online at https://doi.org/10.1016/j.scitotenv.2023.166440.

References

Alfarra, M.R., Prevot, A.S.H., Szidat, S., Sandradewi, J., Weimer, S., Lanz, V.A., Schreiber, D., Mohr, M., Baltensperger, U., 2007. Identification of the mass spectral signature of organic aerosols from wood burning emissions. Environ. Sci. Technol. 41, 5770–5777. https://doi.org/10.1021/es062289b.

Alfoldy, B., Gregorič, A., Ivančič, M., Ježek, I., Rigler, M., 2023. Source apportionment of black carbon and combustion-related CO2 for the determination of source-specific emission factors. Atmos. Meas. Tech. 16, 135–152. https://doi.org/10.5194/amt-2022-53.

Amato, F., Pandolfi, M., Escrig, A., Querol, X., Alastuey, A., Pey, J., Perez, N., Hopke, P. K., 2009a. Quantifying road dust resuspension in urban environment by multilinear engine: a comparison with PMF2. Atmos. Environ. 43, 2770–2780. https://doi.org/10.1016/j.atmosenv.2009.02.039.

Amato, F., Pandolfi, M., Viana, M., Querol, X., Alastuey, A., Moreno, T., 2009b. Spatial and chemical patterns of PM10 in road dust deposited in urban environment. Atmos. Environ. 43, 1650–1659. https://doi.org/10.1016/j.atmosenv.2008.12.009.

Bozzetti, C., Daellenbach, K.R., Hueglin, C., Fermo, P., Sciare, J., Kasper-Giebl, A., Mazar, Y., Abbaszade, G., El Kazzi, M., Gonzalez, R., Shuster-Meiseles, T., Flasch, M., Wolf, R., Křepelová, A., Canonaco, F., Schnelle-Kreis, J., Slowik, J.G., Zimmermann, R., Rudich, Y., Baltensperger, U., El Haddad, I., Prévôt, A.S.H., 2016. Size-resolved identification, characterization, and quantification of primary biological organic aerosol at a European rural site. Environ. Sci. Technol. 50, 3425–3434. https://doi.org/10.1021/acs.est.5b05960.

Bozzetti, C., El Haddad, I., Salameh, D., Daellenbach, K.R., Fermo, P., Gonzalez, R., Minguillón, M.C., Iinuma, Y., Poulain, L., Elser, M., Müller, E., Slowik, J.G., Jaffrezo, J.L., Baltensperger, U., Marchand, N., Prévôt, A.S.H., 2017. Organic aerosol source apportionment by offline-AMS over a full year in Marseille. Atmos. Chem. Phys. 17, 8247–8268. https://doi.org/10.5194/acp-17-8247-2017.

Brines, M., Dall'Osto, M., Amato, F., Minguillón, M.C., Karanasiou, A., Grimalt, J.O., Alastuey, A., Querol, X., van Drooge, B.L., 2019. Source apportionment of urban PM1 in Barcelona during SAPUSS using organic and inorganic components. Environ. Sci. Pollut. Res. 26, 32114–32127. https://doi.org/10.1007/s11356-019-06199-3.

Canonaco, F., Slowik, J.G., Baltensperger, U., Prévôt, A.S.H., 2015. Seasonal differences in oxygenated organic aerosol composition: implications for emissions sources and factor analysis. Atmos. Chem. Phys. 15, 6993–7002. https://doi.org/10.5194/acp-15-6993-2015.

Canonaco, F., Tobler, A., Chen, G., Sosedova, Y., Gates Slowik, J., Bozzetti, C., Rudolf Daellenbach, K., El Haddad, I., Crippa, M., Huang, R.J., Furger, M., Baltensperger, U., Prévôt, A.S.H., 2021. A new method for long-term source apportionment with time-dependent factor profiles and uncertainty assessment using SoFi pro: application to 1 year of organic aerosol data. Atmos. Meas. Tech. 14, 923–943. https://doi.org/10.5194/amt-14-923-2021.

Casotto, R., Cvitešić Kušan, A., Bhattu, D., Cui, T., Manousakas, M.I., Frka, S., Kroflič, A., Grgić, I., Ciglenečki, I., Baltensperger, U., Slowik, J.G., Daellenbach, K.R., Prévôt, A. S.H., 2022. Chemical composition and sources of organic aerosol on the Adriatic coast in Croatia. Atmos. Environ. X 13. https://doi.org/10.1016/j.aeaoa.2022.100159.

Cavalli, F., Putaud, J.P., 2010. Toward a standardized thermal-optical protocol for measuring atmospheric organic and elemental carbon: the eusaar protocol. Atmos. Meas. Tech. 3, 79–89. https://doi.org/10.5194/amtd-2-2321-2009.

Chen, J., Hoek, G., 2020. Long-term exposure to PM and all-cause and cause-specific mortality: a systematic review and meta-analysis. Environ. Int. 143, 105974 https://doi.org/10.1016/j.envint.2020.105974.

Chowdhury, P.H., He, Q., Carmieli, R., Li, C., Rudich, Y., Pardo, M., 2019. Connecting the oxidative potential of secondary organic aerosols with reactive oxygen species in exposed lung cells. Environ. Sci. Technol. 53, 13949–13958. https://doi.org/10.1021/acs.est.9b04449.

Crippa, M., Canonaco, F., Slowik, J.G., El Haddad, I., Decarlo, P.F., Mohr, C., Heringa, M. F., Chirico, R., Marchand, N., Temime-Roussel, B., Abidi, E., Poulain, L., Wiedensohler, A., Baltensperger, U., Prévôt, A.S.H., 2013a. Primary and secondary organic aerosol origin by combined gas-particle phase source apportionment. Atmos. Chem. Phys. 13, 8411–8426. https://doi.org/10.5194/acp-13-8411-2013.

Crippa, M., Decarlo, P.F., Slowik, J.G., Mohr, C., Heringa, M.F., Chirico, R., Poulain, L., Freutel, F., Sciare, J., Cozic, J., Di Marco, C.F., Elsasser, M., Nicolas, J.B., Marchand, N., Abidi, E., Wiedensohler, A., Drewnick, F., Schneider, J., Borrmann, S., Nemitz, E., Zimmermann, R., Jaffrezo, J.L., Prévôt, A.S.H., Baltensperger, U., 2013b. Wintertime aerosol chemical composition and source apportionment of the organic fraction in the metropolitan area of Paris. Atmos. Chem. Phys. 13, 961–981. https://doi.org/10.5194/acp-13-961-2013.

Crippa, M., Canonaco, F., Lanz, V.A., Äijälä, M., Allan, J.D., Carbone, S., Capes, G., Ceburnis, D., Dall'Osto, M., Day, D.A., DeCarlo, P.F., Ehn, M., Eriksson, A., Freney, E., Ruiz, L.H., Hillamo, R., Jimenez, J.L., Junninen, H., Kiendler-Scharr, A., Kortelainen, A.M., Kulmala, M., Laaksonen, A., Mensah, A.A., Mohr, C., Nemitz, E., O'Dowd, C., Ovadnevaite, J., Pandis, S.N., Petäjä, T., Poulain, L., Saarikoski, S., Sellegri, K., Swietlicki, E., Tiitta, P., Worsnop, D.R., Baltensperger, U., Prévôt, A.S.H., 2014. Organic aerosol components derived from 25 AMS data sets across Europe using a consistent ME-2 based source apportionment approach. Atmos. Chem. Phys. 14, 6159–6176. https://doi.org/10.5194/acp-14-6159-2014.

Cusack, M., Alastuey, A., Pérez, N., Pey, J., Querol, X., 2012. Trends of particulate matter (PM 2.5) and chemical composition at a regional background site in the Western Mediterranean over the last nine years (2002−2010). Atmos. Chem. Phys. 12, 8341–8357. https://doi.org/10.5194/acp-12-8341-2012.

Daellenbach, K.R., Bozzetti, C., Křepelová, A., Canonaco, F., Wolf, R., Zotter, P., Fermo, P., Crippa, M., Slowik, J.G., Sosedova, Y., Zhang, Y., Huang, R.J., Poulain, L., Szidat, S., Baltensperger, U., El Haddad, I., Prévôt, A.S.H., 2016. Characterization and source apportionment of organic aerosol using offline aerosol mass spectrometry. Atmos. Meas. Tech. 9, 23–39. https://doi.org/10.5194/amt-9-23-2016.

Daellenbach, K.R., Stefenelli, G., Bozzetti, C., Vlachou, A., Fermo, P., Gonzalez, R., Piazzalunga, A., Colombi, C., Canonaco, F., Hueglin, C., Jaffrezo, J.-L., Bianchi, F., Slowik, J.G., Baltensperger, U., El-Haddad, I.H., Prévôt, A.S., 2017. Long-term chemical analysis and organic aerosol source apportionment at 9 sites in Central Europe: source identification and uncertainty assessment. Atmos. Chem. Phys. 17 https://doi.org/10.5194/acp-2017-124.

Daellenbach, K.R., El-Haddad, I., Karvonen, L., Vlachou, A., Corbin, J.C., Slowik, J.G., Heringa, M.F., Bruns, E.A., Luedin, S.M., Jaffrezo, J.L., Szidat, S., Piazzalunga, A., Gonzalez, R., Fermo, P., Pflueger, V., Vogel, G., Baltensperger, U., Prévôt, A.S.H., 2018. Insights into organic-aerosol sources via a novel laser-desorption/ionization mass spectrometry technique applied to one year of PM10 samples from nine sites in central Europe. Atmos. Chem. Phys. 18, 2155–2174. https://doi.org/10.5194/acp-18-2155-2018.

Daellenbach, K.R., Uzu, G., Jiang, J., Cassagnes, L.E., Leni, Z., Vlachou, A., Stefenelli, G., Canonaco, F., Weber, S., Segers, A., Kuenen, J.J.P., Schaap, M., Favez, O., Albinet, A., Aksoyoglu, S., Dommen, J., Baltensperger, U., Geiser, M., El Haddad, I., Jaffrezo, J.L., Prévôt, A.S.H., 2020. Sources of particulate-matter air pollution and its oxidative potential in Europe. Nature 587, 414–419. https://doi.org/10.1038/s41586-020-2902-8.

DeCarlo, P.F., Kimmel, J.R., Trimborn, A., Northway, M.J., Jayne, J.T., Aiken, A.C., Gonin, M., Fuhrer, K., Horvath, T., Docherty, K.S., Worsnop, D.R., Jimenez, J.L., 2006. Field-deployable, high-resolution, time-of-flight aerosol mass spectrometer. Anal. Chem. 78, 8281–8289. https://doi.org/10.1021/ac061249n.

Decesari, S., Sowlat, M.H., Hasheminassab, S., Sandrini, S., Gilardoni, S., Facchini, M.C., Fuzzi, S., Sioutas, C., 2017. Enhanced toxicity of aerosol in fog conditions in the Po Valley, Italy. Atmos. Chem. Phys. 17, 7721–7731. https://doi.org/10.5194/acp-17-7721-2017.

Delfino, R.J., Staimer, N., Tjoa, T., Arhami, M., Polidori, A., Gillen, D.L., George, S.C., Shafer, M.M., Schauer, J.J., Sioutas, C., 2010. Associations of primary and secondary organic aerosols with airway and systemic inflammation in an elderly panel cohort. Epidemiology 21, 892–902. https://doi.org/10.1097/EDE.0b013e3181f20e6c.

Derwent, R.G., Jenkin, M.E., Utembe, S.R., Shallcross, D.E., Murrells, T.P., Passant, N.R., 2010. Secondary organic aerosol formation from a large number of reactive man-made organic compounds. Sci. Total Environ. 408, 3374–3381. https://doi.org/10.1016/j.scitotenv.2010.04.013.

Drinovec, L., Močnik, G., Zotter, P., Prévôt, A.S.H., Ruckstuhl, C., Coz, E., Rupakheti, M., Sciare, J., Müller, T., Wiedensohler, A., Hansen, A.D.A., 2015. The "dual-spot" Aethalometer: an improved measurement of aerosol black carbon with real-time loading compensation. Atmos. Meas. Tech. 8, 1965–1979. https://doi.org/10.5194/amt-8-1965-2015.

Ealo, M., Alastuey, A., Pérez, N., Ripoll, A., Querol, X., Pandolfi, M., 2017. From air quality to climate; impact of aerosol sources on optical properties at urban, regional and continental levels in the north-western Mediterranean. Atmos. Chem. Phys. Discuss. https://doi.org/10.5194/acp-2017-217.

Ealo, M., Alastuey, A., Pérez, N., Ripoll, A., Querol, X., Pandolfi, M., 2018. Impact of aerosol particle sources on optical properties in urban, regional and remote areas in the North-Western Mediterranean. Atmos. Chem. Phys. 18, 1149–1169. https://doi.org/10.5194/acp-18-1149-2018.

EarthData, 2021. Active Fire Data [WWW Document]. https://www.earthdata.nasa.gov/learn/find-data/near-real-time/firms/active-fire-data.

EC, 2008. DIRECTIVE 2008/50/EC OF THE EUROPEAN PARLIAMENT AND OF THE COUNCIL of 21 may 2008 on ambient air quality and cleaner air for Europe. Off. J. Eur. Union 44.

EC, 2011. Establishing guidelines for demonstration and subtraction of exceedances attributable to natural sources under the Directive 2008/50/EC on ambient air quality and cleaner air for Europe.

Escrig, A., Monfort, E., Celades, I., Querol, X., Amato, F., Minguillón, M.C., Hopke, P.K., 2009. Application of optimally scaled target factor analysis for assessing source contribution of ambient PM10. J. Air Waste Manage. Assoc. 59, 1296–1307. https://doi.org/10.3155/1047-3289.59.11.1296.

Escudero, M., Viana, M., Querol, X., Alastuey, A., Díez Hernández, P., García Dos Santos, S., Anzano, J., 2015. Industrial sources of primary and secondary organic aerosols in two urban environments in Spain. Environ. Sci. Pollut. Res. 22, 10413–10424. https://doi.org/10.1007/s11356-015-4228-x.

Gangoiti, G., Alonso, L., Navazo, M., Albizuri, A., Perez-Landa, G., Matabuena, M., Valdenebro, V., Maruri, M., Antonio García, J., Millán, M.M., 2001. Regional transport of pollutants over the Bay of Biscay: analysis of an ozone episode under a blocking anticyclone in west-central Europe. Atmos. Environ. 36, 1349–1361. https://doi.org/10.1016/S1352-2310(01)00536-2.

Heal, M.R., Kumar, P., Harrison, R.M., 2012. Particles, air quality, policy and health. Chem. Soc. Rev. 41, 6606–6630. https://doi.org/10.1039/c2cs35076a.

Healy, R.M., Sciare, J., Poulain, L., Crippa, M., Wiedensohler, A., Prévôt, A.S.H., Baltensperger, U., Sarda-Estève, R., McGuire, M.L., Jeong, C.H., McGillicuddy, E., O'Connor, I.P., Sodeau, J.R., Evans, G.J., Wenger, J.C., 2013. Quantitative determination of carbonaceous particle mixing state in Paris using single-particle mass spectrometer and aerosol mass spectrometer measurements. Atmos. Chem. Phys. 13, 9479–9496. https://doi.org/10.5194/acp-13-9479-2013.

Healy, R.M., Sofowote, U., Su, Y., Debosz, J., Noble, M., Jeong, C.H., Wang, J.M., Hilker, N., Evans, G.J., Doerksen, G., Jones, K., Munoz, A., 2017. Ambient measurements and source apportionment of fossil fuel and biomass burning black carbon in Ontario. Atmos. Environ. 161, 34–47. https://doi.org/10.1016/j.atmosenv.2017.04.034.

Huang, D.D., Li, Y.J., Lee, B.P., Chan, C.K., 2015. Analysis of organic sulfur compounds in atmospheric aerosols at the HKUST supersite in Hong Kong using HR-ToF-AMS. Environ. Sci. Technol. 49, 3672–3679. https://doi.org/10.1021/es5056269.

Hüser, I., Harder, H., Heil, A., Kaiser, J.W., 2017. Assumptions about footprint layer heights influence the quantification of emission sources: a case study for Cyprus. Atmos. Chem. Phys. 17, 1955–10967. https://doi.org/10.5194/acp-17-10955-2017.

in 't Veld, M., Alastuey, A., Pandolfi, M., Amato, F., Pérez, N., Reche, C., Via, M., Minguillón, M.C., Escudero, M., Querol, X., 2021. Compositional changes of PM2.5 in NE Spain during 2009–2018: a trend analysis of the chemical composition and source apportionment. Sci. Total Environ. 795 https://doi.org/10.1016/j.scitotenv.2021.148728.

in 't Veld, M., Pandolfi, M., Amato, F., Pérez, N., Reche, C., Dominutti, P., Jaffrezo, J., Alastuey, A., Querol, X., Uzu, G., 2023. Discovering oxidative potential (OP) drivers of atmospheric PM10, PM2.5, and PM1 simultaneously in north-eastern Spain. Sci. Total Environ. 857 https://doi.org/10.1016/j.scitotenv.2022.159386.

Jia, Y.Y., Wang, Q., Liu, T., 2017. Toxicity research of PM2.5 compositions in vitro. Int. J. Environ. Res. Public Health 14. https://doi.org/10.3390/ijerph14030232.

Kanakidou, M., Seinfeld, J.H., Pandis, S.N., Barnes, I., Dentener, F.J., Facchini, M.C., Van Dingenen, R., Ervens, B., Nenes, A., Nielsen, C.J., Swietlicki, E., Putaud, J.P., Balkanski, Y., Fuzzi, S., Horth, J., Moortgat, G.K., Winterhalter, R., Myhre, C.E.L., Tsigaridis, K., Vignati, E., Stephanou, E.G., Wilson, J., 2005. Organic aerosol and global climate modelling: a review. Atmos. Chem. Phys. 5, 1053–1123.

Kelly, F.J., Fussell, J.C., 2012. Size, source and chemical composition as determinants of toxicity attributable to ambient particulate matter. Atmos. Environ. 60, 504–526. https://doi.org/10.1016/j.atmosenv.2012.06.039.

Lal, S., Venkataramani, S., Chandra, N., Cooper, O.R., Brioude, J., Naja, M., 2014. Transport effects on the vertical distribution of tropospheric ozone over western India. J. Geophys. Res.-Atmos. 119, 10012–10026. https://doi.org/10.1002/2014JD021854.

Leaitch, W.R., Macdonald, A.M., Brickell, P.C., Liggio, J., Sjostedt, S.J., Vlasenko, A., Bottenheim, J.W., Huang, L., Li, S.M., Liu, P.S.K., Toom-Sauntry, D., Hayden, K.A., Sharma, S., Shantz, N.C., Wiebe, H.A., Zhang, W., Abbatt, J.P.D., Slowik, J.G., Chang, R.Y.W., Russell, L.M., Schwartz, R.E., Takahama, S., Jayne, J.T., Ng, N.L., 2011. Temperature response of the submicron organic aerosol from temperate forests. Atmos. Environ. 45, 6696–6704. https://doi.org/10.1016/j.atmosenv.2011.08.047.

Li, J., Chen, H., Li, X., Wang, M., Zhang, X., Cao, J., Shen, F., Wu, Y., Xu, S., Fan, H., Da, G., Huang, R. jin, Wang, J., Chan, C.K., De Jesus, A.L., Morawska, L., Yao, M., 2019. Differing toxicity of ambient particulate matter (PM) in global cities. Atmos. Environ. 212, 305–315. https://doi.org/10.1016/j.atmosenv.2019.05.048.

Millán, M.M., Salvador, R., Mantilla, E., Kallos, G., 1997. Photooxidant dynamics in the Mediterranean basin in summer: results from European research projects. J. Geophys. Res.-Atmos. 102, 8811–8823. https://doi.org/10.1029/96jd03610.

Millán, M.M., José Sanz, M., Salvador, R., Mantilla, E., 2002. Atmospheric dynamics and ozone cycles related to nitrogen deposition in the western Mediterranean. Environ. Pollut. 118, 167–186. https://doi.org/10.1016/S0269-7491(01)00311-6.

Minguillón, M.C., Perron, N., Querol, X., Szidat, S., Fahrni, S.M., Alastuey, A., Jimenez, J. L., Mohr, C., Ortega, A.M., Day, D.A., Lanz, V.A., Wacker, L., Reche, C., Cusack, M., Amato, F., Kiss, G., Hoffer, A., Decesari, S., Moretti, F., Hillamo, R., Teinilä, K., Seco, R., Peñuelas, J., Metzger, A., Schallhart, S., Müller, M., Hansel, A., Burkhart, J. F., Baltensperger, U., Prévôt, A.S.H., 2011. Fossil versus contemporary sources of fine elemental and organic carbonaceous particulate matter during the DAURE campaign in Northeast Spain. Atmos. Chem. Phys. 11, 12067–12084. https://doi.org/10.5194/acp-11-12067-2011.

Minguillón, M.C., Ripoll, A., Pérez, N., Prévôt, A.S.H., Canonaco, F., Querol, X., Alastuey, A., 2015. One year ACSM at Montseny regional background site chemical characterization of submicron regional background aerosols in the Western Mediterranean using an aerosol chemical speciation monitor. Atmos. Chem. Phys. 15, 6379–6391. https://doi.org/10.5194/acp-15-6379-2015.

Mohr, C., DeCarlo, P.F., Heringa, M.F., Chirico, R., Slowik, J.G., Richter, R., Reche, C., Alastuey, A., Querol, X., Seco, R., Peñuelas, J., Jiménez, J.L., Crippa, M., Zimmermann, R., Baltensperger, U., Prevot, A.S.H., 2012. Identification and quantification of organic aerosol from cooking and other sources in Barcelona using aerosol mass spectrometer data. Atmos. Chem. Phys. 12, 1649–1665. https://doi.org/10.5194/acp-12-1649-2012.

Mukherjee, A., Agrawal, M., 2017. World air particulate matter: sources, distribution and health effects. Environ. Chem. Lett. 15, 283–309. https://doi.org/10.1007/s10311-017-0611-9.

Norris, G., Duvall, R., Brown, S., Bai, S., 2014. EPA Positive Matrix Factorization (PMF) 5.0 Fundamentals and User Guide [WWW Document]. EPA.

Paatero, P., 1999. The multilinear engine—a table-driven, least squares program for solving multilinear problems, including the n-way parallel factor analysis model. J. Comput. Graph. Stat. 8, 854–888. https://doi.org/10.1080/10618600.1999.10474853.

Pandolfi, M., Martucci, G., Querol, X., Alastuey, A., Wilsenack, F., Frey, S., O'Dowd, C.D., Dall'Osto, M., 2013. Continuous atmospheric boundary layer observations in the coastal urban area of Barcelona during SAPUSS. Atmos. Chem. Phys. 13, 4983–4996. https://doi.org/10.5194/acp-13-4983-2013.

Pandolfi, M., Querol, X., Alastuey, A., Jimenez, J.L., Jorba, O., Day, D., Ortega, A., Cubison, M.J., Comerón, A., Sicard, M., Mohr, C., Prevot, A.S.H., Minguillón, M.C., Pey, J., Baldasano, J.M., Burkhart, J.F., Seco, R., Peñuelas, J., van Drooge, B.L., Artiñano, B., Di Marco, C., Nemitz, E., Schallhart, S., Metzger, A., Hansel, A., Lorente, J., Ng, S., Jayne, J., Szidat, S., 2014. Effects of sources and meteorology on particulate matter in the Western Mediterranean Basin: an overview of the DAURE campaign. J. Geophys. Res. 119, 4978–5010. https://doi.org/10.1002/2013JD021079.

Pandolfi, M., Alastuey, A., Pérez, N., Reche, C., Castro, I., Shatalov, V., Querol, X., 2016. Trends analysis of PM source contributions and chemical tracers in NE Spain during 2004-2014: a multi-exponential approach. Atmos. Chem. Phys. 16, 11787–11805. https://doi.org/10.5194/acp-16-11787-2016.

Park, M., Joo, H.S., Lee, K., Jang, M., Kim, S.D., Kim, I., Borlaza, L.J.S., Lim, H., Shin, H., Chung, K.H., Choi, Y.H., Park, S.G., Bae, M.S., Lee, J., Song, H., Park, K., 2018. Differential toxicities of fine particulate matters from various sources. Sci. Rep. 8, 1–11. https://doi.org/10.1038/s41598-018-35398-0.

Pérez, N., Pey, J., Castillo, S., Viana, M., Alastuey, A., Querol, X., 2008. Interpretation of the variability of levels of regional background aerosols in the Western Mediterranean. Sci. Total Environ. 407, 527–540. https://doi.org/10.1016/j.scitotenv.2008.09.006.

Pey, J., Querol, X., Alastuey, A., 2009. Variations of levels and composition of PM10 and PM2.5 at an insular site in the Western Mediterranean. Atmos. Res. 94, 285–299. https://doi.org/10.1016/j.atmosres.2009.06.006.

Pey, J., Pérez, N., Querol, X., Alastuey, A., Cusack, M., Reche, C., 2010. Intense winter atmospheric pollution episodes affecting the Western Mediterranean. Sci. Total Environ. 408, 1951–1959. https://doi.org/10.1016/j.scitotenv.2010.01.052.

Pieber, S.M., El Haddad, I., Slowik, J.G., Canagaratna, M.R., Jayne, J.T., Platt, S.M., Bozzetti, C., Daellenbach, K.R., Fröhlich, R., Vlachou, A., Klein, F., Dommen, J., Miljevic, B., Jiménez, J.L., Worsnop, D.R., Baltensperger, U., Prévôt, A.S.H., 2016. Inorganic salt interference on CO2+ in aerodyne AMS and ACSM organic aerosol composition studies. Environ. Sci. Technol. 50, 10494–10503. https://doi.org/10.1021/acs.est.6b01035.

Pisso, I., Sollum, E., Grythe, H., Kristiansen, N.I., Cassiani, M., Eckhardt, S., Arnold, D., Morton, D., Thompson, R.L., Groot Zwaaftink, C.D., Evangeliou, N., Sodemann, H., Haimberger, L., Henne, S., Brunner, D., Burkhart, J.F., Fouilloux, A., Brioude, J., Philipp, A., Seibert, P., Stohl, A., 2019. The Lagrangian particle dispersion model FLEXPART version 10.4. Geosci. Model Dev. 12, 4955–4997. https://doi.org/10.5194/gmd-12-4955-2019.

Qi, L., Vogel, A.L., Esmaeilirad, S., Cao, L., Zheng, J., Jaffrezo, J.L., Fermo, P., Kasper-Giebl, A., Daellenbach, K.R., Chen, M., Ge, X., Baltensperger, U., Prévôt, A.S.H., Slowik, J.G., 2020. A 1-year characterization of organic aerosol composition and sources using an extractive electrospray ionization time-of-flight mass spectrometer (EESI-TOF). Atmos. Chem. Phys. 20, 7875–7893. https://doi.org/10.5194/acp-20-7875-2020.

Querol, X., Alastuey, A., Rodriguez, S., Plana, F., Ruiz, C.R., Cots, N., Massagué, G., Puig, O., 2001. PM10 and PM2.5 source apportionment in the Barcelona metropolitan area, Catalonia, Spain. Atmos. Environ. 35, 6407–6419. https://doi.org/10.1016/S1352-2310(01)00361-2.

Querol, X., Alastuey, A., Ruiz, C.R., Artiñano, B., Hansson, H.C., Harrison, R.M., Buringh, E., Ten Brink, H.M., Lutz, M., Bruckmann, P., Straehl, P., Schneider, J., 2004a. Speciation and origin of PM10 and PM2.5 in selected European cities. Atmos. Environ. 38, 6547–6555. https://doi.org/10.1016/j.atmosenv.2004.08.037.

Querol, X., Alastuey, A., Viana, M.M., Rodriguez, S., Artiñano, B., Salvador, P., Garcia Do Santos, S., Fernandez Patier, R., Ruiz, C.R., De La Rosa, J., Sanchez De La Campa, A., Menendez, M., Gil, J.I., 2004b. Speciation and origin of PM10 and PM2.5 in Spain. J. Aerosol Sci. 35, 1151–1172. https://doi.org/10.1016/j.jaerosci.2004.04.002.

Querol, X., Alastuey, A., Moreno, T., Viana, M.M., Castillo, S., Pey, J., Rodríguez, S., Cristóbal, A., Jiménez, S., Pallarés, M., de la Rosa, J., Artíñano, B., Salvador, P., Sánchez, M., García Dos Santos, S., Herce Garraleta, M.D., Fernández-Patier, R., Moreno-Grau, S., Negral, L., Minguillón, M.C., Monfort, E., Sanz, M.J., Palomo-Marín, R., Pinilla-Gil, E., Cuevas, E., 2006. Atmospheric particulate matter in Spain: levels, composition and source origin. doi:10.13140/2.1.3948.5440.

Querol, X., Viana, M., Alastuey, A., Amato, F., Moreno, T., Castillo, S., Pey, J., de la Rosa, J., Sánchez de la Campa, A., Artíñano, B., Salvador, P., García Dos Santos, S., Fernández-Patier, R., Moreno-Grau, S., Negral, L., Minguillón, M.C., Monfort, E., Gil, J.I., Inza, A., Ortega, L.A., Santamaría, J.M., Zabalza, J., 2007. Source origin of trace elements in PM from regional background, urban and industrial sites of Spain. Atmos. Environ. 41, 7219–7231. https://doi.org/10.1016/j.atmosenv.2007.05.022.

Querol, X., Alastuey, A., Pey, J., Cusack, M., Pérez, N., Mihalopoulos, N., Theodosi, C., Gerasopoulos, E., Kubilay, N., Koçak, M., 2009. Variability in regional background aerosols within the Mediterranean. Atmos. Chem. Phys. 9, 4575–4591. https://doi.org/10.5194/acp-9-4575-2009.

Querol, X., Alastuey, A., Viana, M., Moreno, T., Reche, C., Minguillón, M.C., Ripoll, A., Pandolfi, M., Amato, F., Karanasiou, A., Pérez, N., Pey, J., Cusack, M., Vázquez, R., Plana, F., Dall'Osto, M., De La Rosa, J., Sánchez De La Campa, A., Fernández-Camacho, R., Rodríguez, S., Pio, C., Alados-Arboledas, L., Titos, G., Artíñano, B., Salvador, P., García Dos Santos, S., Fernández Patier, R., 2013. Variability of carbonaceous aerosols in remote, rural, urban and industrial environments in Spain: implications for air quality policy. Atmos. Chem. Phys. 13, 6185–6206. https://doi.org/10.5194/acp-13-6185-2013.

Querol, X., Alastuey, A., Pandolfi, M., Reche, C., Pérez, N., Minguillón, M.C., Moreno, T., Viana, M., Escudero, M., Orio, A., Pallarés, M., Reina, F., 2014. 2001-2012 trends on air quality in Spain. Sci. Total Environ. 490, 957–969. https://doi.org/10.1016/j.scitotenv.2014.05.074.

Ripoll, A., Minguillón, M.C., Pey, J., Pérez, N., Querol, X., Alastuey, A., 2015. Joint analysis of continental and regional background environments in the western Mediterranean: PM1 and PM10 concentrations and composition. Atmos. Chem. Phys. 15, 1129–1145. https://doi.org/10.5194/acp-15-1129-2015.

Rodríguez, S., Querol, X., Alastuey, A., Mantilla, E., 2002. Origin of high summer PM10 and TSP concentrations at rural sites in eastern Spain. Atmos. Environ. 36, 3101–3112. https://doi.org/10.1016/S1352-2310(02)00256-X.

Sandradewi, J., Prévôt, A.S.H., Szidat, S., Perron, N., Alfarra, M.R., Lanz, V.A., Weingartner, E., Baltensperger, U.R.S., 2008. Using aerosol light abosrption measurements for the quantitative determination of wood burning and traffic emission contribution to particulate matter. Environ. Sci. Technol. 42, 3316–3323. https://doi.org/10.1021/es702253m.

Seco, R., Peñuelas, J., Filella, I., Llusià, J., Molowny-Horas, R., Schallhart, S., Metzger, A., Müller, M., Hansel, A., 2011. Contrasting winter and summer VOC mixing ratios at a forest site in the Western Mediterranean Basin: the effect of local biogenic emissions. Atmos. Chem. Phys. 11, 13161–13179. https://doi.org/10.5194/acp-11-13161-2011.

Srivastava, D., Daellenbach, K.R., Zhang, Y., Bonnaire, N., Chazeau, B., Perraudin, E., Gros, V., Lucarelli, F., Villenave, E., Prévôt, A.S.H., El Haddad, I., Favez, O., Albinet, A., 2021. Comparison of five methodologies to apportion organic aerosol sources during a PM pollution event. Sci. Total Environ. 757 https://doi.org/10.1016/j.scitotenv.2020.143168.

Stohl, A., Burkhart, J.F., Eckhardt, S., Hirdman, D., Sodemann, H., 2007. An Integrated Internet-Based System for Analyzing the Influence of Emission Sources and Atmospheric Transport on Measured Concentrations of Trace Gases and Aerosols. Kjeller.

Van Drooge, B.L., Garatachea, R., Reche, C., Titos, G., Alastuey, A., Lyamani, H., Alados-Arboledas, L., Querol, X., Grimalt, J.O., 2022. Primary and secondary organic winter aerosols in Mediterranean cities under different mixing layer conditions (Barcelona and Granada). Environ. Sci. Pollut. Res. 29, 36255–36272. https://doi.org/10.1007/s11356-021-16366-0/Published.

Via, M., Minguillón, M.C., Reche, C., Querol, X., Alastuey, A., 2021. Increase of secondary organic aerosol over four years in an urban environment. Atmos. Chem. Phys. 1–20.

Viana, M., Reche, C., Amato, F., Alastuey, A., Querol, X., Moreno, T., Lucarelli, F., Nava, S., Calzolai, G., Chiari, M., Rico, M., 2013. Evidence of biomass burning aerosols in the Barcelona urban environment during winter time. Atmos. Environ. 72, 81–88. https://doi.org/10.1016/j.atmosenv.2013.02.031.

Vlachou, A., Daellenbach, K.R., Bozzetti, C., Chazeau, B., Salazar, G.A., Szidat, S., Jaffrezo, J.L., Hueglin, C., Baltensperger, U., El Haddad, I., Prévôt, A.S.H., 2018. Advanced source apportionment of carbonaceous aerosols by coupling offline AMS and radiocarbon size-segregated measurements over a nearly 2-year period. Atmos. Chem. Phys. 18, 6187–6206. https://doi.org/10.5194/acp-18-6187-2018.

WHO, 2021. WHO "Global Air Quality Guidelines" Organization.

Yáñez-Serrano, A.M., Bach, A., Bartolomé-Català, D., Matthaios, V., Seco, R., Llusià, J., Filella, I., Peñuelas, J., 2021. Dynamics of volatile organic compounds in a western Mediterranean oak forest. Atmos. Environ. 257 https://doi.org/10.1016/j.atmosenv.2021.118447.

Yus-Díez, J., Bernardoni, V., Močnik, G., Alastuey, A., Ciniglia, D., Ivančič, M., Querol, X., Perez, N., Reche, C., Rigler, M., Vecchi, R., Valentini, S., Pandolfi, M., 2021. Determination of the multiple-scattering correction factor and its cross-sensitivity to scattering and wavelength dependence for different AE33 Aethalometer filter tapes: a multi-instrumental approach. Atmos. Meas. Tech. 14, 6335–6355. https://doi.org/10.5194/amt-14-6335-2021.

Zhang, H., Li, Z., Liu, Y., Xinag, P., Cui, X.Y., Ye, H., Hu, B.L., Lou, L.P., 2018a. Physical and chemical characteristics of PM2.5 and its toxicity to human bronchial cells BEAS-2B in the winter and summer. J Zhejiang Univ Sci B 19, 317–326. https://doi.org/10.1631/jzus.B1700123.

Zhang, W., Lin, S., Hopke, P.K., Thurston, S.W., van Wijngaarden, E., Croft, D., Squizzato, S., Masiol, M., Rich, D.Q., 2018b. Triggering of cardiovascular hospital admissions by fine particle concentrations in New York state: before, during, and after implementation of multiple environmental policies and a recession. Environ. Pollut. 242, 1404–1416. https://doi.org/10.1016/j.envpol.2018.08.030.

Zięba, A., Ramza, P., 2011. Standard deviation of the mean of autocorrelated observations estimated with the use of the autocorrelation function estimated from the data. Metrol. Measurement Syst. 18, 529–542. https://doi.org/10.2478/v10178-011-0052-x.

Zotter, P., El-Haddad, I., Zhang, Y., Hayes, P.L., Zhang, X., Lin, Y.H., Wacker, L., Schnelle-Kreis, J., Abbaszade, G., Zimmermann, R., Surratt, J.D., Weber, R., Jimenez, J.L., Szidat, S., Baltensperger, U., Prévôt, A.S.H., 2014. Diurnal cycle of fossil and nonfossil carbon using radiocarbon analyses during CalNex. J. Geophys. Res. 119, 6818–6835. https://doi.org/10.1002/2013JD021114.